UNIVERSITEIT VAN PRETORIA
UNIVERSITY OF PRETORIA
YUNIBESITHI YA PRETORIA

MATHEMATICAL MODELLING OF FLOW DOWNSTREAM OF AN ORIFICE UNDER FLOW-ACCELERATED CORROSION

by

Conrad Sanama

Submitted in partial fulfilment of the requirements for the degree

MASTER OF SCIENCE (Mechanical Engineering)

in the

Faculty of Engineering, Built Environment and Information Technology

University of Pretoria

2017

© University of Pretoria

ABSTRACT

Title: Mathematical modelling of flow downstream of an orifice under flow-accelerated corrosion

Student: Conrad Sanama

Supervisors: Prof Mohsen Sharifpur and Prof Josua Meyer

Department: Mechanical and Aeronautical Engineering

University: University of Pretoria

Degree: Master of Science (Mechanical Engineering)

The main objective of this work is to establish an analytical model to evaluate the rate of corrosion in a horizontal pipe downstream of an orifice under flow-accelerated corrosion (FAC). FAC is a serious issue in nuclear and fossil power plants. In this work, an experimental setup was built to observe the effect of the flow on corrosion inside a tube. The experiments confirmed that the flow inside the tube caused more corrosion. However, accurate experimental data from literature has been selected and correlated by dimensional analysis, the modelling method of repeating variables and the Buckingham Pi theorem. It was found that the Sh number and the relative distance from the orifice are the main dimensionless parameters influencing FAC downstream of an orifice. The maximum value of the FAC rate could be well-predicted for the OR of 0.25, while the location of the maximum FAC rate could be well predicted for the OR of 0.5. The maximum FAC rate occurs between 2D to 4D downstream of the orifice and increases with a decreasing OR. This work could be useful for professionals in industry and researchers in the field and could be the starting point for a new way of evaluating the FAC rate downstream of a flow's singularity.

Keywords: Flow-accelerated corrosion, orifice, mathematical modelling

© University of Pretoria

STATEMENT OF SOURCES

I hereby declare that the work presented in this dissertation is, to the best of my knowledge and belief, original, except as acknowledged in the text. I also state that the material contained herein has not been previously submitted, either in whole or in part, for a degree at the University of Pretoria, or any other university.

……...

Conrad Sanama

……day of ……year……

© University of Pretoria

ACKNOWLEDGEMENT

Thanks are due to those who supported this dissertation; particularly to my supervisor, Prof Mohsen Sharifpur, for his guidance. I am also indebted to Prof Josua Meyer, together with my supervisor, for their financial and materials support through the Clean Energy Research Group at the University of Pretoria.

I must also thank my peers from the Department of Mechanical and Aeronautical Engineering at the University of Pretoria.

Most importantly, I extend my gratitude to my family and friends who supported me throughout this process.

© University of Pretoria

CONTENTS

Table of contents

© University of Pretoria

© University of Pretoria

© University of Pretoria

LIST OF FIGURES

© University of Pretoria

LIST OF TABLES

© University of Pretoria

LIST OF ACRONYMS

BWR	Boiling water reactor
CFD	Computational fluid dynamics
FAC	Flow-accelerated corrosion
CR	Corrosion rate (mm/day)
EC	Erosion corrosion
MTC	Mass transfer coefficient
OR	Orifice ratio
PWR	Pressurised water reactor
SiC	Silicon carbide
SRET	Scanning reference electrode technique
ENMs	Electrochemical noise measurements
Re	Reynolds number
S_c	Schmidt number
Sh	Sherwood number
Fr	Froude number
Eu	Euler number
L	Liter

© University of Pretoria

m	Metre
s	Second
u	Fluid velocity (m/s)
ρ	Fluid density (kg/m^3)
Γ	Diffusion coefficient
mm	Millimetre
ppb	Parts-per billion
ASTM G1	American Society for Testing and Materials G1
μ	Fluid dynamic viscosity (mPa.s)
D	Mass diffusivity
d_o	Distance from orifice (mm)
d	Orifice diameter (mm)
d_H	Hydraulic diameter (mm)
pH	Potential of hydrogen
O	Oxygen
d_p	Pipe diameter (mm)
ΔP	Pressure difference (Pa)
ΔT	Temperature change (^{o}C)

© University of Pretoria

g	Gravitational force (m/s^2)
C	Concentration of species (mol/l)
mol	Mole
T	Temperature
o_C	Degre Celsius
mV_p	Millivolt
Pa	Pascal
mPa	Millipascal
kg	Kilogram

© University of Pretoria

UNIVERSITEIT VAN PRETORIA
UNIVERSITY OF PRETORIA
YUNIBESITHI YA PRETORIA

PUBLICATIONS IN JOURNALS AND CONFERENCE PROCEEDINGS

Articles in peer-reviewed journals:

Sanama, C., Sharifpur, M., Meyer, J. P., "Mathematical modelling of flow downstream of an orifice under flow-accelerated corrosion", submitted to *Nuclear Engineering and Design*.

© University of Pretoria

UNIVERSITEIT VAN PRETORIA
UNIVERSITY OF PRETORIA
YUNIBESITHI YA PRETORIA

CHAPTER 1:

INTRODUCTION TO THE RESEARCH PROBLEM

© University of Pretoria

1.1 BACKGROUND OF THE STUDY

Corrosion in the context of corrosion engineering is the reaction of an engineering constructional metal with its environment with a consequent deterioration in the properties of the metal (Shreir, Jarman and Burstein 1994). Therefore, for corrosion to occur, a metal, an environment and the interface between the metal and the environment are needed. In most cases, corrosion occurs when the environment in contact with the metal is moving, which might result in an increase or decrease of the corrosion rate (Shreir et al. 1994). When the moving environment is a fluid and increases the degradation of the metal, the process is often referred to as flow-induced corrosion. A special case of flow-induced corrosion is flow-accelerated corrosion (FAC), which is a degradation of the metal that causes a thinning of the walls of the pipes due to the fluid flow (El-Gammal, Mazhar, Cotton, Shefski, Pietralik and Ching 2010). FAC occurs when the metal reacts with oxygen at the metal oxide interface (El-Gammal, Ahmed and Ching 2012) to form a protective layer (magnetite) (Petric and Ksiazek 1997) as the fluid is flowing. The protective layer dissolves in water, becomes thin and enhances the transfer of mass from the wall to the bulk of flow within the diffusion boundary layers (Ahmed, Bello, El Nakla and Al Sarkhi 2012).

1.2 MATHEMATICAL MODELLING AND EXPERIMENTS

Mathematical modelling has become a great tool in engineering over the years. It refers to the use of mathematics to describe real engineering phenomena (Sarmasti 2011). Mathematical modelling helps to establish relations between the different parameters that influence a process and has the advantage of reducing cost and time in analysing or designing a process. Ale (1981; 1986) summarises the modelling of a problem as follows:

© University of Pretoria

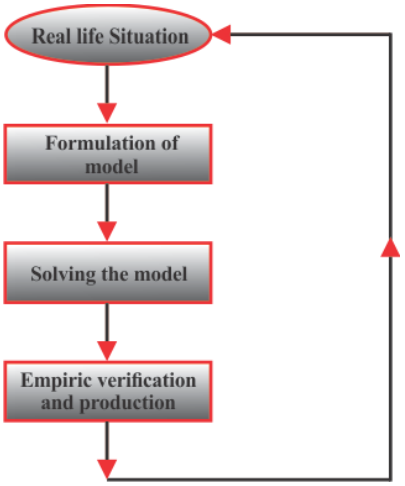

Figure 1: Idealisation of a problem into a model (Ale 1986)

Nevertheless, experiments have always been a good way to check the validity of a model. Although experiments may be time-consuming and expensive to run, it is good to rely on them to avoid mistakes in design or the analysis of a process. Therefore, it is of great importance to set up an experiment to evaluate the effect of flow on corrosion inside a pipe, as this will contribute to the observation of this phenomenon. Experiments enable the researcher to objectively observe phenomena that are made to occur. The phenomena are represented by independent variables. When the researcher runs an experiment, some parameters are set and the outcome is observed. Everything is then based on both observation and the ability of the researcher to interpret the observations using the data collected and plots, which may lead to an empirical formula or a useful correlation later on.

In this work, the mathematical model is based on a dimensionless model obtained using the Buckingham Pi theorem method. The result obtained from the model is compared to the results of the experiments.

1.3 PROBLEM STATEMENT

© University of Pretoria

FAC damages have been reported since 1981 (Kastner, Ervem Henzel and Stellwag 1990), but the problem was brought up after a rupture in a condensate line at the Surry Nuclear Power Plant in 1986 (Petric and Ksiazek 1997). In 1999, an extensive steam leakage from the rupture of the shell-side of a feed water heater at the Point Beach Power Plant in the USA was reported (Yurmanov and Rakhmanov 2009). FAC is higher in components such as orifices, valves, expansions or contractions, tees and elbows due to an important change in the direction of the flow and instabilities downstream of these flow singularities. Several research papers have been published in recent years to evaluate metal loss due to FAC in these components, but nothing consistent has been published to explain metal loss due to FAC in straight pipes in the case of single- and two-phase flow. In June 1987, FAC occurred not only in elbows, but also in straight pipes at Trepan (Kastner et al. 1990). There was a lack of modelling of corrosion-controlled mass transfer near the wall. Numerous empirical approaches have been offered to predict the rate of mass transfer between phases in flowing fluids, but a thorough understanding of the fundamental transfer mechanism in single-phase flow through modelling to analyse pipe corrosion is necessary. For instance, the modelling of a phenomenon like the effect of bubbles mixed with the single-phase flow on pipe corrosion has not been well examined, which makes it of great interest to explore. This is because piping systems are common in many industries.

1.4 OBJECTIVE OF THE RESEARCH

This work is based on the application of known mathematical and experimental techniques to resolve an industrial problem. The practical aim of this work is to improve the existing mathematical modelling of corrosion in pipes and to establish a correlation to evaluate the rate of corrosion of pipes through which water flows.

1.5 RESEARCH PLAN

© University of Pretoria

This dissertation consists of six chapters and an appendix, as described below:

- **Chapter 1** provides an overview of the phenomenon of corrosion in pipes with a specific description of FAC. The concept of mathematical modelling is introduced, as well as the importance of an experimental setup. In this section, the scope and aims of the dissertation are also presented.
- **Chapter 2** presents a review of previously completed works.
- **Chapter 3** details the modelling of corrosion in pipes, which relates to mass transfer from the solid wall.
- **Chapter 4** presents the experimental setup and the experimental results.
- **Chapter 5** presents the results from the flow modelling and details the interpretation of the results.
- **Chapter 6** presents the conclusion and makes recommendations.
- A complete list of references is given.
- The appendix provides the derivation of the equations.

© University of Pretoria

CHAPTER 2:

LITERATURE REVIEW

© University of Pretoria

2.1 INTRODUCTION

In their work entitled "Relation between mass transfer and corrosion in a turbulent pipe flow", Sydberger and Lotz (1982) stated that the acceleration of corrosion attack due to the high flow rate of a liquid medium can either be due to the mechanical removal of corrosion products or to mass transfer effects. In practice, most corrosion attacks are due to diffusion. An example is the corrosion of carbon steel exposed to natural water, which occurs as a result of the flux of oxygen towards the metal or rust surface. The corrosion of copper alloys at a low flow rate has been reported to be dominated by the diffusion of copper ions far from the metal surface (Sydberger and Lotz 1982). Under conditions of a low flow rate, a protective layer of corrosion products is formed, which might be dissolved at high flow rates of the same medium. An experiment conducted by Bianchi, Fiori, Longhi and Mazza (1978) demonstrated that the "horseshoe", a typical indication of erosion-corrosion (EC), might be reproduced under the condition of pure mass transfer control by dissolving samples of benzoic acid without erosion effect. The formation of the corrosion product is due to mass transfer at the surface of the metal. The magnitude at the metal-liquid interface is sometimes necessary for the creation of passivating films (Sydberger and Lotz 1982).

Postlethwaite, Dobbin and Bergevin (1985) state that the metal loss of carbon steel piping carrying slurry was mostly due to corrosion controlled by the mass transfer of oxygen, and that the role of the solid particles was to prevent the formation of a protective layer that would reduce the loss rate. Lotz and Postlethwaite (1990) and Postlethwaite et al. (1985) found the surface roughness, as well as an increase in turbulence within the mass transfer layer, to be the factors governing the mass transfer of oxygen.

FAC and EC are similar material degradation processes. Confusion exists between these two processes as they are both forms of corrosion that involve the removal of a protective layer

© University of Pretoria

(erosive effect) and the acceleration of metal loss due to a flowing fluid or impingement (Schweitzer 2007).

The difference between these two processes lies in the way the protective layer is removed. In EC, the protective layer is mechanically removed, usually by a secondary phase (dispersed phase) like a solid particle in liquid, bubbles and water droplets. The wall shear stresses that occur in single-phase flow are too small to allow an important removal of corrosion products.

When the oxide or protective layer is not removed mechanically, but is dissolved, allowing the metal to corrode, it is referred to as FAC (Robinson and Drews 1999). FAC is thus corrosion-controlled mass transfer between the protective oxide layer and the unsaturated flowing fluid. It therefore appears to be important to analyze mass transfer from the solid wall to the fluid stream in both one-phase and two-phase water-air flow. This is because mass transfer plays an important role in the loss rate of the material in both FAC and EC.

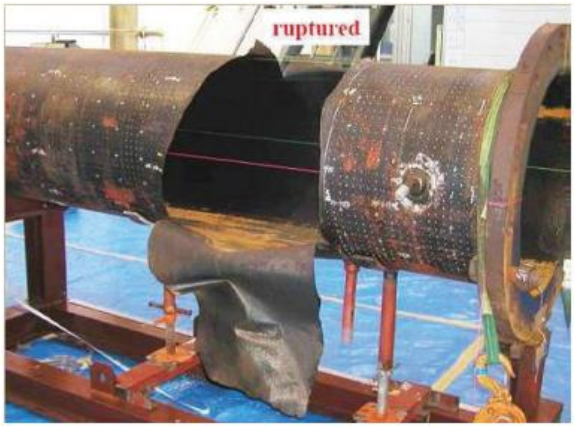

Figure 2: Mihama pressurised water reactor (Uchida 2006)

Figure 3: Surry pressurised water reactor (Poulson, Greenwell, Chexal and Horowitz 1992)

Table 1. Examples of FAC in nuclear power plants

Plant		Component	Parameters				
			T (°C)	pH	O	d (mm)	R_e
2	Mihama PWR	Condensate water pipe after orifice d/d_o = 1 612	140–142	8.6–9.3	<5 ppb	540	5.8×10^6
3	Surry PWR	90° bend after reducing T-piece in condensate system	190	8.9–9.0	4 ppb	305	10^7 (approximately)

© University of Pretoria

2.2 CORROSION MEASUREMENT

The scanning reference electrode technique (SRET) is an electrochemical technique that enables one to locate the position of localised corrosion. The technique has the advantage of keeping the ongoing corrosion processes and the corrosion rate unchanged. The development of corrosion attack and the corrosion rate can be monitored by SRET. The use of SRET has been reported to analyse the pitting attack of stainless steels of Type 304 in a ferric chloride (Isaacs and Vyas 1981). A number of active pits were a function of surface preparation and time. Impingement of the coupon of steel into the solution results in a rapid increase in the potential of the coupon above the pitting potential. The active pits were generated and grew with time while the potential of the coupon was decreased. The small potential increase was reported after the re-passivation of the pits, and SRET enabled the separation of re-passivated and active pits. The results were consistent with the changes in the original oxide layer over the pit before the pitting attack. The protection of the growing pit was greater with thicker oxide (Isaacs and Vyas 1981). Pitting corrosion for AISI 304L stainless steel pipe was evaluated by Wharton and Wood (2004), they used hydrodynamic and electrochemical noise measurements (ENMs) for a range of flow regimes from laminar to turbulent. Metastable pitting was evident under all flow regimes and stable pit growth was more evident during laminar flow immediately before the transition to turbulent flow (Wharton and Wood 2004). Tousek (1981) investigated the time and potential dependence of localised corrosion in iron to improve knowledge regarding the mechanism of localised corrosion. The potentiodynamic and potentio-static methods for the measurement of localised corrosion were used. The curves in potentiodynamic polarisation were obtained at a rate of $10\, mV_p s^{-1}$. The potentio-static methods require one to set the potential above the breakdown potential 10 minutes after the passivation of the electrode. The number of pits was tracked, along with the time dependence of localized corrosion. The data collected enabled the

© University of Pretoria

researcher to calculate and derive equations for the current density in the pits for various environments.

Tong (1979) investigated the electrochemical and corrosion behaviour of Carpenter 20 Cb-3 alloy, Type 304 and Type 316 stainless steels, in 99% sulfuric acid at temperatures up to 127 ^{o}C. The rate of corrosion was measured by weight loss according to the American Society for Testing and Materials G1 (ASTM G1) standard. Before corrosion measurement, the coupons were polished with silicon carbide (SiC) paper rinsed in water, immersed in acetone and dried. The corrosion morphology of the coupon was shown after 48 hours of testing by means of optical microscopy. The rate of corrosion increased with temperature and iron concentration in the acid solution. Type 304 stainless steel exhibited general corrosion at 30 ^{o}C and 74 ^{o}C. Carpenter 20 Cb-3 alloy and Type 316 stainless steels exhibited general corrosion at 30 ^{o}C and combined intergranular and general corrosion attacks at 74 ^{o}C. Pitting corrosion was noticed for all three alloys at 127 ^{o}C. Turnbull and Robinson (2005) investigated the corrosion behaviour of the historic vessel *SL Dolly* that had been immersed in the Ullswater Lake in Cumbria for over 67 years. The vessel had undergone very low corrosion degradation. Coupons were made from the A106 steel and wrought iron samples. The coupons were degreased, pre-weighed and immersed in tap water in open topped 2 L troughs. An adequate design for air supply was designed for one trough containing three similar coupons. A second trough with the same number of coupons was filled with non-aerated tap water so that oxygen diffusion only occurred from the surface. A third trough contained a de-aerated mixture of pre-washed fine silica sand and tap water to simulate the condition of the *SL Dolly*'s boiler when covered with sediment (Turnbull and Robinson 2005). The coupons were exposed for three months, and measurements were made according to the ASTM G1 standard. The low corrosion rate of the vessel was found to be mainly due to the low conductivity of the water and the low oxygen content of the water (Turnbull and Robinson 2005). The corrosion rate of wrought iron was between 0.018 and 0.030

© University of Pretoria

mm a year for a metal loss of 1.2–2.0 mm over the 67 years (Turnbull and Robinson 2005). The corrosion rates of wrought iron were found to be quite similar to those of modern boiler steel (Turnbull and Robinson 2005).

The influence of pH, immersion time and chloride ion concentration on the corrosion rate of friction-stir-welded AZ61A magnesium alloys was investigated by Dhanagal, Rajendra and Balasubramanian (2012). The researchers used a AZ61A magnesium alloy plate with dimensions of 300 mm × 150 mm × 6 mm for the analysis. The joint was fabricated according to Dhanagal et al. (2012). The coupons were immersed in a solution prepared with 5 g barium nitrate ($Ba(NO_3)_2$) + 50 g chromium trioxide (CrO_3) + 2.5 g silver nitrate ($AgNO_3$) with 250 ml distilled water for 60 seconds. The corrosion was measured according to the ASTM G1 standard, and the corrosion rate was calculated from the ASTM G31 formulation. Metallographic analysis was realised on the coupons using a light-optical microscope. The corrosion products were analysed using XRD and SEM-EDAX analysis. The corrosion rate was found to be high for the acid solution at given concentrations and immersion times. The increase in chloride ion concentrations resulted in an important corrosion attack, as well as an increase in the corrosion rate of the AZ61A magnesium alloy welds. By increasing the immersion time, the corrosion resistance of the AZ61A magnesium alloy welds was increased, and the formation of hydroxide films to reduce further degradation of the material was possible (Dhanagal et al. 2012).

Liang, Deng, Xie, Gomez, Hu, Zhang, Ong and Adin (2013) prepared cast iron coupons of 40 mm × 13 mm × 2 mm with a 5 mm diameter hole at one end to investigate the impact of the flow rate on the corrosion of cast iron. The coupons were inserted in transparent pipes of 25 mm ID and 150 mm in length. Liang et al. (2013) used water containing $Ca(OH)_2$ + $MgCO3$ + CO_2 + $NaHCO_3$ necessary for the re-mineralisation of seawater reverse osmosis (SWRO) water. The flow rate was set at 1 L per day, 10 L per day or 20 L per day using peristaltic pumps. Each test

© University of Pretoria

was run over 22 days, and the samples were analysed according to the ASTM G1 standard. The coupon samples were cleaned with cold tap water to remove the corrosion layers and then immersed in an appropriate chemical solution (500 ml HCl + 3.5 g $(CH_2)_6$ N_4). This was followed by water rinsing and oven drying, as well as surface polishing with Grit paper. Scanning electron microscopy (SEM) and the INCA X-act were used to observe the microstructure of the rusting and to analyze the chemical composition. The rate of corrosion increased with the flow rate as the path of oxygen diffusion within the laminar layer at the metal surface decreased (Liang et al. 2013). This was confirmed after cleaning the rough surfaces of the coupon tested at a high flow rate. Lepidocrocite was noticed as the principal substance in the rusting. Calcium crystal fibre deposition led to less material degradation, and the water had a yellow appearance due to the rusting.

2.3 PARAMETERS GOVERNING FLOW-ACCELERATED CORROSION

Poulson (1999) found factors such as the orientation of the piping component, the piping material and the fluid temperature to be the governing factors of FAC. On the other hand, Chen, McLaury and Shirazi (2005) identified mass transfer at the wall, turbulence close to the wall and wall shear stresses as the governing hydrodynamic factors responsible for FAC. Kim, Park, Kojasoy Kelly and Marshall (2007) found hydrodynamic parameters controlling FAC in two-phase (liquid-gas) flows to be more complex than for single-phase flows. This is due to the interactions between the liquid turbulence structure and the gas phase, as well as phase redistribution. The FAC rate is a function of the mass flux of ferrous ions when the flow effects are important; the mass flux is a function of the mass transfer coefficient (MTC) and a variation of the concentration within the boundary layer; while MTC is a strong function of the surface geometry, but also of the roughness, flow rate, local turbulence, void fraction in a situation of

© University of Pretoria

two-phase flow, and the physical properties of the transported species and of the water (Pietralik and Schefski 2009 (a,b,c)).

Table 2. Parameters influencing FAC and measurement techniques

Parameter	Measuring techniques	References
Velocity (u)	1. Calculated from flow rate and flow area 2. Ultrasonic sensor 3. Pitot tube	Poulson 1983 Hewitt 1978 Massey 2006
Reynolds number (R_e)	Calculated from velocity, the diameter of the tube, kinematic viscosity.	
MTC requirements: • Use of realistic geometries • Measurements of both smooth and rough surfaces • Use in two-phase flow	1. Dissolution of sparingly soluble solid 2. Limiting current 3. Analogy with heat transfer 4. Computational	Poulson 1987 Wraag 1977 Wang 2012

2.4 MODELLING OF FLOW-ACCELERATED CORROSION

© University of Pretoria

Nesic and Postlethwaite (1991) analysed the effects of disturbed flow on EC due to mass transfer using a numerical simulation of turbulent flow in a sudden expansion. Their model was good at predicting the loss rate of carbon steel. They related mass transfer to turbulence near the wall; in the presence of rust, film fluctuations affect both mass transfer and the mechanical removal of the film. In a situation where corrosion is driven by mass transfer, Keating and Nesic (1999) affirmed that the wall's MTC and corrosion rate can be related to each other. Keating and Nesic (1999) modelled two-phase liquid-particle flow and investigated the effects of such a flow on mass transfer in a 180˚ bend. They found the bend orientation to have a significant effect on the particle motion. They observed that the maximum mechanical removal of materials was at the extrados on the side walls close to the outlet of the bend. Velocity seems to be the most important parameter governing FAC in multiphase flow. This is regarding the work done by Bozzini, Ricotti, Boniardi and Mele (2003) who numerically analysed the effects of the four-phase flow of two immiscible liquids, gas and solid particles on EC. Davis and Frawley (2009) used a computational model to evaluate FAC rate and validated against experimental results for a contracting-expanding geometry. They found that in order to accurately predict FAC wear, the independent grids of Sherwood number (S_h number) were required in providing a new metric to evaluate turbulent FAC modelling (Davis and Frawley 2009). Ma, Ferng and Ma (1998) numerically simulated two-phase steam-liquid flow in various bend configurations. The predicted critical FAC locations and those obtained from plant measurements were in good agreement. They also found that the critical FAC locations were mostly at the pipe bend layout. The accurate prediction of mass transfer near the wall requires one to resolve the mass transfer boundary layer, which may be an order of magnitude smaller than the viscous sublayer (Ahmed et al. 2012).

© University of Pretoria

Table 3. Examples of the use of computational fluid dynamics (CFD) in FAC studies

Authors	Purpose	Comments	References
Uchida, Naitoh, Uehara and Lister	Prediction of FAC with Mihama as test case	No comparison with existing data and its extrapolation to a high Re or effects of roughness.	Uchida, Naitoh, Uehara and Lister 2007
Pietralik and Smith	Prediction/explaining CANDU feeder FAC	Compares with some but not all bend data. Attempts to deal with roughness development and component interactions.	Pietralik and Smith 2006
Pietralik and Schefski			Pietralik and Schefski 2009 (a,b,c)
Nesic and Postlethwaite	Prediction of erosion-corrosion following sudden expansion	Makes key point that profiles of MTC and shear stress do not correlate.	Nesic and Postlethwaite 1991
Zinemans and Herszaz	Prediction of FAC in bifurcation and nozzle	Limited detail to check results, but claims there is agreement; effects of roughness not considered.	Zinemans and Herszaz 2008
Yoneda	Predict FAC in PWR and boiling water reactor (BWR) of 45° elbow	Interesting, but again no comparison with others or the effects of roughness.	Yoneda 2009

2.5 EXPERIMENTAL INVESTIGATION OF FLOW-ACCELERATED CORROSION

Poulson (1999) conducted an experimental study of FAC degradation in 180˚ bends under single-phase and two-phase air/water flow. FAC was considerable along the intrados in the

© University of Pretoria

single-phase condition, while it was significant along the extrados in the two-phase annular flow. Ahmed (2010), from his investigation of 211 inspection data points of 90˚ elbows in carbon steel at several nuclear power plants, indicated a significant increase in the wear rate of about 70% due to proximity. He also showed, during the same year, that FAC is higher in components such as orifices, valves, expansions or contractions, tees and elbows. This is due to an important change in the direction of the flow and instabilities downstream from these flow singularities. Four years earlier, Chen et al. (2005) had identified piping elbows as one of the most common components affected by FAC. The carbon dioxide corrosion behavior of API N80 grade steel enhanced by gas-liquid two-phase vertical upward slug flow has been experimentally investigated by Zheng, Che and Liu (2008); they found that alternated wall shear stress direction, wall normal stress fluctuation and mass transfer near the wall have significant effects on the corrosion process of carbon dioxide. Flow in 90˚ bends undergoes changes in the flow direction, resulting in the development of flow separation and/or secondary flows (El-Gammal, Ahmed and Ching 2012). A pressure drop along the elbow is created by secondary flows and increases the wall shear stresses and the flow turbulence near the wall. Yamagata, Ito, Sato and Fujisawa (2014) experimentally investigated the mass transfer characteristics in a pipe behind an orifice. Their measurement of mass transfer coefficient was performed by using benzoic acid dissolution method in a flow of water. Their result showed a maximum S_h number downstream of the orifice in the region of 1 to 2 pipe diameters that gradually decreases further downstream which was in line with the results found in the previous works.

2.6 MASS TRANSFER FROM SOLID TO LIQUID IN THE PIPE

Reynolds was the first to describe the analogy between momentum and mass transfer. He postulated the exact similarity between momentum exchange and material exchange (Lin, Moulton and Putnam 1953). This is only correct when the Schmidt number (S_c number) tends to

© University of Pretoria

unity. Prandtl (1928) and Taylor (1916, 1917) included a laminar mass transfer boundary near the wall in the analogy at all values of the S_c number. Von Karman (1939), Boelter, Martinelli and Jonassen (1941), Reichardt (1943), Linton and Sherwood (1950) analysed the problem more extensively by the velocity distribution measurements in straight tubes. The fluid was divided into a sublaminar layer, a buffer region and the turbulent core. The transfer of matters in the sublaminar layer is by molecular motion only because there is no turbulence or eddy diffusion. The simultaneous action of the eddy and molecular diffusion control the mass transfer and velocity distribution in the buffer region. Velocity distribution and mass transfer are determined by the eddy diffusion of momentum and mass in the turbulent core layer. Lin et al. (1953) stated that the concept of the existence of a sublaminar layer for molecular diffusion might not be true. They defended their statement from ultramicroscopic observations of fluid particles on the wall by Fage and Townend (1932), revealing the existence of a vertical component to the wall of the velocity fluctuations that is cancelled only at the vicinity of the wall. Unfortunately, a few eddies near the wall could not be expressed quantitatively. However, the small eddies become traceable when the diffusivity coefficients of the materials are low. Levich (1962), by analogy with the laminar diffusion, attempted to offer the magnitude of the diffusion sublayer in terms of the thickness of the sublaminar layer and the S_c number, where the mass transfer between the diffusion sublayer and the sublaminar layer is due to turbulence, even though the viscous mechanism is the driving force of momentum transfer. The analysis was intriguing, but was crude and lacked supporting experimental evidence (Lin et al. 1953). Harriott and Hamilton (1965) have measured the mass transfer rates for smooth pipe sections of benzoic acid dissolving in glycerine-water solutions; the data were correlated and compared with published correlations, this resulted with the exponent (0.346) for the S_c number appearing to be significantly different from the value 1/3 predicted by simple theories.

© University of Pretoria

2.7 THE EFFECT OF TWO-PHASE FLOW ON PIPE CORROSION

Bubbles can have a significant effect on the hydrodynamics factors that govern FAC, as they can have an important effect on the wall shear stress and pressure (Ahmed et al. 2012). Jepson (1989) found that high-velocity slugs can cause high shear forces and turbulence at the pipe wall. This might contribute to the mechanical removal of the protective film. Ahmed, Bello and Nakla (2014) experimentally studied the effect of two-phase flow on FAC downstream of an orifice. The FAC wear of carbon steel piping was simulated experimentally by circulating air-water mixtures through hydrocal test sections at a liquid R_e number, $R_e = 20\,000$, and different air mass flow rates (Ahmed et al. 2014). The maximum FAC wear was found to occur at approximately two to five pipe diameters downstream of the orifice. The obtained results were found to be consistent with the single-phase flow case (Ahmed et al. 2014). FAC was found to depend on the relative values of the mixture mass quality and the volumetric void fraction. FAC rates were obtained for higher values of mass quality (Ahmed et al. 2014).

2.8 CORRELATIONS

There appears to be reasonably widespread agreement that the basic mechanism of FAC is the enhanced transportation of dissolved ferrous ions away from the metal surface. This causes the protective magnetite film to be thinned down and results in essentially linear kinetics. This can be compared to parabolic kinetics during normal corrosion (Poulson 2014).

The simplest formulation of a FAC model gives the corrosion rate as the product of the MTC and the solubility driving force (ΔC), where ΔC is the difference between the solubility and the bulk solution level (Poulson 2014).

Because the FAC rate is proportional to the MTC within the boundary layer, it is of great importance to evaluate this coefficient. MTC non-dimensional representation is given by

© University of Pretoria

$S_h = \frac{MTC.d_H}{D}$ with S_h as the Sherwood number, d_H as the hydraulic diameter of the pipe and D as the mass diffusivity coefficient. By means of dimensional analysis and experiments, some authors have attempted to relate this MTC to the Re and S_c numbers, but there is still a lack of accuracy in these correlations (Berger and Hue 1977; Poulson and Robinson 1988; Poulson 2014).

2.9 CONCLUSION

FAC is mainly due to diffusion. The difference between FAC and EC is that in FAC, the protective layer is dissolved rather than removed. This allows the metal to corrode. Various methods have also been found to measure the rate of corrosion of a metal. The weight loss method seems to be more practical to execute than the other methods. Mass transfer, turbulence close to the wall and wall shear stress are the hydrodynamic factors that cause FAC. Piping orientation and materials, as well as fluid temperature, are important parameters that influence FAC. An analysis of FAC is mainly done with computational tools and various numerical simulations, such as the numerical simulation of turbulent flow in a sudden expansion that has been recorded in the literature. FAC has been investigated experimentally and recorded in the literature in 180˚ and 90˚ bends. An exact similarity between momentum exchange and mass exchange has also been reported. In the situation of a two-phase flow, the wall shear stress, pressure and turbulence close to pipe wall can cause the protective layer to be removed, and hence FAC to be enhanced. In two-phase flow, FAC enhancement is also subject to mixture quality and void fraction. It is possible to correlate the FAC rate by using the non-dimensional S_h number, which is a function of the MTC and can also be given in terms of R_e and S_c numbers.

© University of Pretoria

UNIVERSITEIT VAN PRETORIA
UNIVERSITY OF PRETORIA
YUNIBESITHI YA PRETORIA

CHAPTER 3:

FLOW AND CORROSION MODELLING DOWNSTREAM OF AN ORIFICE

© University of Pretoria

3.1 FUNDAMENTALS OF FLUID FLOW MODELLING

In this section, the governing equations are stated.

3.1.1 CONSERVATION EQUATIONS

The mathematical descriptions of fluid flow are based on general conservation laws. If one introduces a general variable Φ, the conservative form of all fluid flow equations, including equations for scalar quantities, such as temperature and pollutant concentration, can usefully be written in the following form:

$$\frac{\partial(\rho\Phi)}{\partial t} + div(\rho\Phi u) = div(\Gamma grad\Phi) + S_\Phi \qquad (1)$$

Equation 1 is the so-called transport equation for the property. It clearly highlights the various transport processes: the rate of change term and the convective term on the left-hand side and the diffusive term (Γ = diffusion coefficient) and the source term on the right-hand side.

CONSERVATION OF MASS

From the general form of the conservation equation, the conservation of mass or continuity equation can be obtained by setting $\Phi = 1$.

$$\frac{\partial\rho}{\partial t} + \frac{\partial(\rho u_j)}{\partial x_j} = 0 \qquad (2)$$

There is no source term because mass cannot be created or destroyed.

For incompressible flow, ρ is assumed to be constant and:

$$\frac{\partial(\rho u_j)}{\partial x_j} = 0 \qquad (3)$$

© University of Pretoria

CONSERVATION OF MOMENTUM

$$\frac{\partial(\rho u_i)}{\partial t} + \frac{\partial(\rho u_j u_i)}{\partial x_j} = \frac{\partial}{\partial x_j}\left(\mu \frac{\partial u_i}{\partial x_j}\right) - \frac{\partial P}{\partial x_i} \quad (4)$$

where μ = viscosity

CONSERVATION OF SPECIES

$$\frac{\partial(\rho C)}{\partial t} + \frac{\partial(\rho u_j C)}{\partial x_j} = \frac{\partial}{\partial x_j}\left(\frac{\mu}{S_c}\frac{\partial C}{\partial x_j}\right) \quad (5)$$

where S_c = Schmidt number

3.2 CORROSION MODELLING

The FAC process in carbon steel piping is described by four steps. In the first step, metal oxidation occurs at the metal-oxide interface in oxygen-free water, and is explained by the following reactions:

$$F_e + 2H_2O \rightarrow F_e^{2+} + 2OH^- + H_2 \quad (6)$$

$$F_e^{2+} + 2OH^- \rightarrow F_e(OH)_2 \quad (7)$$

$$3F_e + 4H_2O \rightarrow F_{e_3}O_4 + 4H_2 \quad (8)$$

The second step involves the solubility of ferrous species through the porous oxide layer into the main water flow. This transport across the oxide layer is controlled by concentration diffusion. The third step is described by the dissolution of magnetite at the oxide-water interface as explained by the following reaction:

$$\frac{1}{3}F_{e_3}O_4 + (2-b)H^+ + \frac{1}{3}H_2 \leftrightarrow F_e(OH)_b^{(2-b)+} + \left(\frac{4}{3} - b\right)H_2O \quad (9)$$

where $F_e(OH)_b^{(2-b)+}$ represents the different ferrous ion species $b = (0, 1, 2, 3)$.

© University of Pretoria

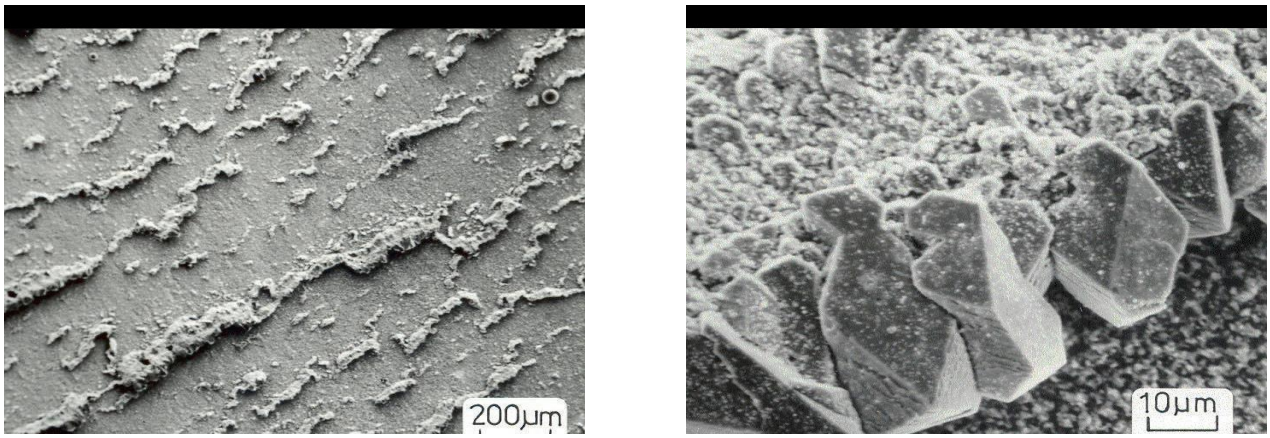

Figure 4. Typical magnetite deposit (Poulson 2014)

In the fourth step, a diffusion process takes place where the ferrous ions transfer into the bulk flowing water across the diffusion boundary layer. In this process, the species migrate from the metal-oxide interface. The species that are dissolved at the oxide-water interface diffuse rapidly into the flowing water. In this case, the concentration of ferrous ions in the bulk water is very low compared to the concentration at the oxide-water interface.

One will notice that the FAC mechanism involves the convective mass transfer of the ferrous ions in the water. The convective mass transfer for single-phase flow is known to be dependent on the hydrodynamic parameters near the wall interface, such as flow velocity, local turbulence, geometry and surface roughness. Over a limited length of the piping component, the FAC rate is considered to be a direct function of the mass flux of ferrous ions and can be calculated from the convective MTC in the flowing water. The FAC rate is then calculated from the MTC and the difference between the concentration of ferrous ions at the oxide-water interface (C_w) and the concentration of a ferrous ion in the bulk of water (C_b) is:

$$FAC\ rate = MTC\ (C_w - C_b) \tag{10}$$

© University of Pretoria

3.3 MODELLING OF THE MASS TRANSFER COEFFICIENT UNDER CONDITION OF FLOW-ACCELERATED CORROSION

The non-dimensional representation of the MTC is:

$$S_h = \frac{MTC.d_H}{D} \tag{11}$$

where d_H is the hydraulic diameter, D is the diffusion coefficient of iron in the water and S_h is the non-dimensional Sherwood number.

Experimentally:

$$S_h = a.R_e^b.S_c^c \tag{12}$$

where a, b and c can be found experimentally.

3.4 THEORY OF SINGLE-PHASE FLOW DOWNSTREAM OF AN ORIFICE

The flow through a thin orifice (Figure 5a) is restricted, causing a negligible loss of kinetic energy, and reaches an area called the vena contracta, downstream of which the flow expands.

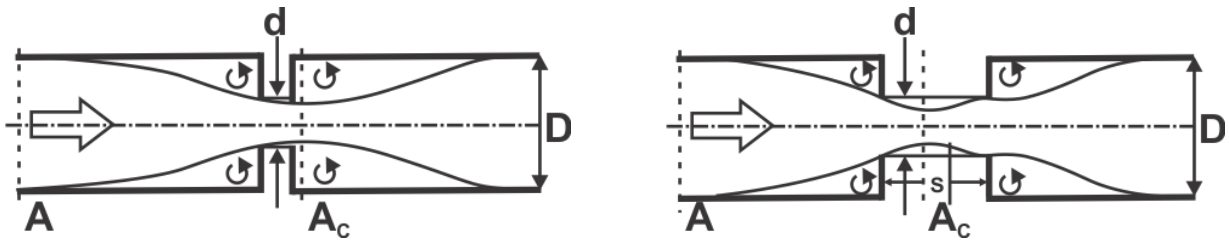

(a) **(b)**

Figure 5. Description of a thin (a) and thick orifice (b)

For flow through a thick orifice (Figure 5b), the flow is parallel at the vena contracta located inside the contraction area, and then expands. For thin and thick orifices, Manmatha and Sukanta (2012) observed a separated flow at the edges of the orifice that reattaches downstream of the

© University of Pretoria

vena contracta. The pressure drop decreases with an increase in the orifice thickness to diameter ratio. This is because the recirculation length increases as the thickness of the orifice decreases, creating more vortices.

3.5 THE FUNDAMENTALS OF NON-DIMENSIONAL ANALYSIS

Dimensional analysis is used to simplify complex engineering problems by combining the key variables of the problems into a compact form that is easy to investigate; this is the so-called similarity (Ain 2001). Dimensional analysis is the best approach for solving problems that are not formulated or bounded. Experiments are simplified because of fewer and specific testing parameters as a result of dimensional analysis.

Dimensional analysis can be segmented according to the following steps:

- **Step 1:** Define the independent variables to be taken into consideration during the analysis.
- **Step 2:** Define the dimension of each independent variable.
- **Step 3:** Formulate the dimensionless variables that are made of independent variables.

3.6 NON-DIMENSIONAL ANALYSIS OF THE CORROSION RATE

By identifying the FAC rate as $CR\ \left(\frac{mm}{day}\right)$, from the literature and the above equations, it is clear that the corrosion rate (CR) is a function of the fluid velocity, fluid density, fluid viscosity, mass diffusivity, the concentration of oxygen in the air, the diameter of the pipe, the diameter of the orifice, pressure change, the temperature variation between the fluid and the wall surface and the gravitational force.

Therefore:

$$CR = f(u, \rho, \mu, D, d_o, C, d_p, \Delta P, \Delta T, g) \tag{13}$$

© University of Pretoria

where the primary dimensions of each parameter are listed below:

CR = Corrosion rate $\{CR\} = \{Lt^{-1}\}$ or $\{CR\} = \{L^2t^{-1}\}$

u = Fluid velocity with $\{u\} = \{Lt^{-1}\}$

ρ = Fluid density with $\{\rho\} = \{ML^{-3}\}$

μ = Fluid viscosity with $\{\mu\} = \{ML^{-1}t^{-1}\}$

D = Mass diffusivity with $\{D\} = \{L^2t^{-1}\}$

d_o = Distance from orifice $\{d_o\} = \{L\}$

C = Concentration of species with $\{C\} = \{NL^{-3}\}$

d_p = Pipe diameter $\{d_p\} = \{L\}$

ΔP = Pressure difference $\{\Delta P\} = \{Mt^{-2}L^{-1}\}$

ΔT = Temperature variation $\{\Delta T\} = \{T\}$

g = Gravitational force $\{g\} = \{Lt^{-2}\}$

With five primary dimensions and the method of repeating variables, the reduction is chosen as $j = 6$, which implies that six π_S' groups have to be established and defined as follows:

$$\pi_1 = f(\pi_2, \pi_3, \pi_4, \pi_5, \pi_6) \tag{14}$$

with

π_1 = Dependent π group

$\pi_2 \ldots \pi_6$ = Independent π groups

© University of Pretoria

3.7 DETERMINATION OF THE π GROUPS

Selecting d_p, u , ρ , C and ΔT as the repeating variables and $\{CR\} = \{Lt^{-1}\}$:

$$\{\pi_1\} = \left\{CR d_p^{a_1} u^{b_1} \rho^{c_1} C^{d_1} (\Delta T)^{e_1}\right\} \tag{15}$$

then,

$$\pi_1 = \frac{CR}{u} \tag{16}$$

$$\{\pi_2\} = \left\{\mu d_p^{a_2} u^{b_2} \rho^{c_2} C^{d_2} (\Delta T)^{e_2}\right\} \tag{17}$$

then,

$$\pi_2 = \frac{\mu}{\rho u d_p} = \frac{1}{R_e} \tag{18}$$

$$\{\pi_3\} = \left\{D d_p^{a_3} u^{b_3} \rho^{c_3} C^{d_3} (\Delta T)^{e_3}\right\} \tag{19}$$

then,

$$\pi_3 = \frac{D}{u d_p} = \frac{1}{S_h} \tag{20}$$

$$\{\pi_4\} = \left\{d_o d_p^{a_4} u^{b_4} \rho^{c_4} C^{d_4} (\Delta T)^{e_4}\right\} \tag{21}$$

then,

$$\pi_4 = \frac{d_o}{d_p} \tag{22}$$

$$\{\pi_5\} = \left\{\Delta P d_p^{a_5} u^{b_5} \rho^{c_5} C^{d_5} (\Delta T)^{e_5}\right\} \tag{23}$$

then,

© University of Pretoria

$$\pi_5 = \frac{\Delta P}{\rho u^2} = Eu \tag{24}$$

$$\{\pi_6\} = \left\{g d_p^{a_6} u^{b_6} \rho^{c_6} C^{d_6} (\Delta T)^{e_6}\right\} \tag{25}$$

then,

$$\pi_6 = \frac{g D_p}{u^2} \cong \frac{u}{\sqrt{g d_p}} = F_r \tag{26}$$

yields to the following function:

$$\frac{CR}{u} = f\left(\frac{1}{R_e}, \frac{1}{S_h}, \frac{d_o}{d_p}, Eu, F_r\right) \tag{27}$$

3.8 CONCLUSION

The analysis of FAC is governed by a transport equation for the property inclusive of the rate of change term, convective term, diffusive term and source term. The FAC process is described by metal oxidation, the solubility of the ferrous species into the main water flow, and the dissolution of magnetite at the oxide-water interface, a diffusion that takes place where the ferrous ions transfer into the bulk flowing water across the diffusion boundary layer. The non-dimensional representation of the MTC is given as a function of the S_h number but is also experimentally evaluated as a function of the R_e and S_c numbers. The difference between the flow downstream of a thick and a thin orifice can be explained by the fact that the flow is parallel at the vena contracta for a thick orifice, while it is restricted through a thin orifice, causing negligible loss of kinetic energy; the pressure drop also decreases with increasing orifice thickness. The non-dimensional analysis introduces its benefits for problems that are not formulated or bounded by simplifying the experiment and limiting the test to specific parameters. The FAC rate can be expressed as a function of 10 parameters. Using the method of repeating variables combined to

© University of Pretoria

the Buckingham Pi theorem, the FAC rate is given as a function of the dimensionless parameters, such as the S_h number.

3.9 RECOMMENDATIONS

From this study, it should be noted that gravity and the difference in pressure ΔP were not taken into consideration. However, in the case of vertical flow, both gravity and the pressure difference would have a considerable effect on the flow, and must therefore be considered.

© University of Pretoria

UNIVERSITEIT VAN PRETORIA
UNIVERSITY OF PRETORIA
YUNIBESITHI YA PRETORIA

CHAPTER 4:

EXPERIMENTAL ANALYSIS

© University of Pretoria

4.1 EXPERIMENTAL SETUP

Experiments were conducted in a flow loop, shown schematically in Figure 6. The apparatus was set up in such a way as to allow for the replacement of the test section after each experiment. Water was drawn from a 100 L tank through a centrifugal pump (rotational pump speed) driven by an electric motor. The flow rate was adjusted by the opening and closing of a gate valve located on the water flow line, but could also be changed by altering the rotational pump speed. The water flow rate was measured using a turbine flow meter. The temperature was measured using thermocouples placed at various locations along the flow loop. The pressure drop was obtained using a differential pressure transducer, which measures the pressure at the inlet and outlet of the test section. Experiments were performed using 6D mm straight tubing. A straight section of pipe of approximately 200D mm was placed upstream of the test section to ensure fully developed inlet flow conditions. An additional straight section of 100D mm was installed downstream of the test section. Special care was taken to reduce the effects of the connections between the test section and the rest of the elements of the flow loop. The test section was made of mild steel with an inner diameter of 50 mm, with a wall thickness of 2 mm. Each test was done with tap water running through the test section for one hour. After each run, the test section was removed from the flow loop and cut axially as shown by the sample's image in Figure 7 (b) to observe the inner surface with a microscope. Afterwards, the sample was taken out, dried, cleaned and weighed to calculate the CR. Subsequently, the specimen was rinsed according to the ASTM G1 standard with a forceful stream of cold tap water to remove residual test solution and loose corrosion products. Before measuring the corrosion, the coupons were polished with SiC paper, rinsed with water, immersed in acetone and dried. The exposure time, weight loss, surface area exposed and density of the metal were used to calculate the CR (Gasem 2011), of the metal using the following formula:

© University of Pretoria

$$P.R.(mm/y) = \frac{mass\ loss\ (g) * 8.76.10^4}{density\left(\frac{g}{cm^3}\right) * area(cm^2) * exposure\ time(hr)} \quad (28)$$

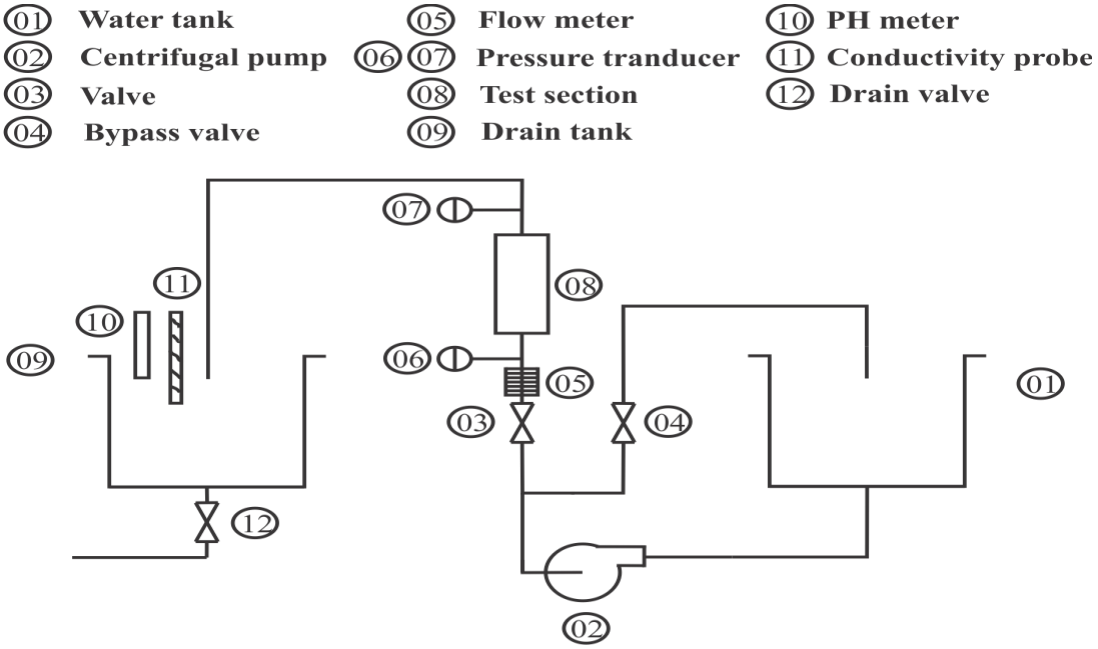

Figure 6. Experimental setup

4.2 EXPERIMENTAL RESULTS

The chronological steps during the experiment were as follows:

- Each experiment was run over one hour.
- The temperature and pressure data were collected each second.
- The calibration curve relating the water electrical conductivity to the amount of dissolved mild steel (conductivity against concentration by volume) was obtained, as well as the determination of the saturation point of mild steel concentration in water, at which the water electrical conductivity remains constant at high mild steel concentration.
- The electric conductivity of the water was recorded before running the test and was considered as the reference conductivity.

© University of Pretoria

- The water conductivity at the exit tank was recorded every two minutes during each test.
- The curve water electrical conductivity against time was obtained and compared to the curve electrical conductivity against concentration by volume.
- The curve concentration by volume against time was obtained to keep track of the increase of the dissolved mild steel in water with time.
- The pH of the water was recorded before running the test and was taken as the reference pH.
- The pH of the water at the exit tank was recorded every two minutes during each test and compared to the variation of water conductivity.
- The curve concentration by volume against pH was to be obtained, as well as the curve pH against time to investigate the contribution of the pH in the experiment.

Figure 7 (a) shows the image of the experimental setup designed and built in the laboratory. This setup could allow running the test at various flow rates by increasing or reducing the rotational speed of the water pump. The flow rate can also be controlled by manually adjusting the valve located upstream of the test section. The pressure transducers were located at the inlet and outlet of the test section, and the date was recorded every 10 minutes. The thermocouples were located at the inlet and outlet of the test section, but also at the inner and outer surface of the test sections so that any eventual change of temperature could be easily recorded. The experimental setup could also be used to run experiments when the test section was heated by a heating element that could be attached all around the outer surface of the test section and connected to the thermocouple to record the change in temperature. The acrylic tubes upstream and downstream of the test section were used to ensure fully developed flow, as well as to monitor the flow of water, especially to avoid the creation of bubbles due to any presence of oxygen along the flow loop.

© University of Pretoria

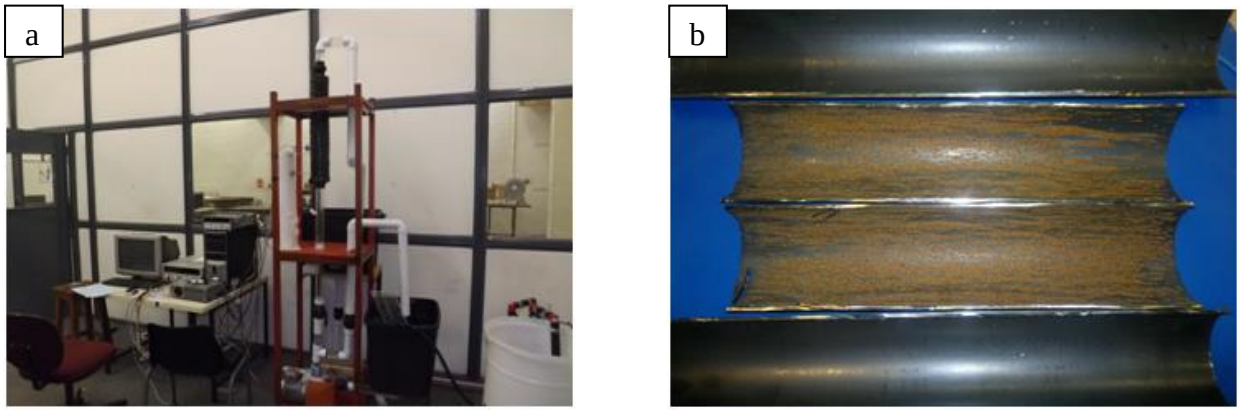

Figure 7 (a) Experimental setup showing test sample, (b) image of test samples

Figure 7 (b) shows an image of the cross-section of the test sample after running an experiment for one hour. Corrosion is clearly observed on the inside surface of the pipe and characterised by an orange-like colour. The corrosion attack appears to diminish, eventually disappearing as the flow moves away from the pipe orifice at the inlet. Attempts to correlate the corrosion of the inside surface of the pipe to the measured electrical conductivity of the water or the pH level were inconclusive. The method of weighing loss was considered. However, due to the round surface of the pipe, many relevant details of that analysis would have been misunderstood.

4.3 CONCLUSION

The experiments were conducted in a closed loop. The test section was made of mild steel because of its fast corrosion particularity. The measurement of the CR by weight loss was found to be problematic due to the geometry of the pipe samples (a hollow cylinder). As a result of overwhelming challenges encountered while experimentally simulating the corrosion of the inside surface of a pipe in the laboratory, which leads to inconclusive results, a selection of previously published experimental data was used to validate the developed correlation.

© University of Pretoria

4.4 RECOMMENDATIONS

The experimental study was done based on visual observation due to the lack of availability of a standard method to test the CR of a pipe in the laboratory. The above experimental setup requires improvements to allow the measurement of the CR so that flow parameters and metal loss due to corrosion can be correlated with better accuracy.

© University of Pretoria

UNIVERSITEIT VAN PRETORIA
UNIVERSITY OF PRETORIA
YUNIBESITHI YA PRETORIA

CHAPTER 5:

RESULTS AND INTERPRETATIONS

© University of Pretoria

5.1 SUMMARY OF THE DIMENSIONAL ANALYSIS

To introduce a new model, let us consider the following:

$$\frac{CR}{u} = f\left(\frac{1}{R_e}, \frac{1}{S_h}, \frac{d_o}{d_p}, Eu, F_r\right) \tag{29}$$

It is possible to neglect Eu, F_r as the gravitation and static pressure are of minor consequences in this analysis, therefore, one can consider:

$$\frac{CR}{u} = f\left(\frac{1}{R_e}, \frac{1}{S_h}, \frac{d_o}{d_p}\right) \tag{30}$$

Now one attempts to build a function as per the above non-dimensional mathematical model:

$$\frac{CR}{u} = (R_e)^{-a}(S_h)^{-b}\left(\frac{d_o}{d_p}\right)^{c} \tag{31}$$

by applying the data from the study proposed by Ahmed et al. (2012) for an orifice ratio (OR) of 0.25 and 0.5.

Note: $u = 0.71\frac{m}{s}$ and $R_e = 20000$

5.2 RESULTS FOR AN ORIFICE RATIO OF 0.25

$$\frac{CR}{u} = (R_e)^{-2.2779}(S_h)^{+1.0871}\left(\frac{d_o}{d_p}\right)^{-1.3662} \quad \text{For} \quad \frac{d_o}{d_p}\ \varepsilon\ [0; 3.4] \tag{32}$$

$$\frac{CR}{u} = (R_e)^{+0.9567}(S_h)^{-1.6254}\left(\frac{d_o}{d_p}\right)^{-7.1168} \quad \text{For} \quad \frac{d_o}{d_p}\ \varepsilon\ [3.4; 6.5] \tag{33}$$

5.3 RESULTS FOR AN ORIFICE RATIO OF 0.5

$$\frac{CR}{u} = k(R_e)^{-2.6560}(S_h)^{+1.1016}\left(\frac{d_o}{d_p}\right)^{0.2063} \quad \text{For} \quad \frac{d_o}{d_p}\ \varepsilon\ [0; 6.5] \tag{34}$$

with $k = 8.5$.

© University of Pretoria

5.4 GENERIC MODEL

$$\frac{CR}{u} = \left[\frac{OR - 0.5}{-0.25}\right](R_e)^{-2.2779}(S_h)^{+1.0871}\left(\frac{d_o}{d_p}\right)^{-1.3662} + k\left[\frac{OR - 0.25}{0.25}\right](R_e)^{-2.6560}(S_h)^{+1.1016}\left(\frac{d_o}{d_p}\right)^{0.2063} \quad (35)$$

for $\frac{d_o}{d_p}$ ε [0; 3.4].

$$\frac{CR}{u} = \left[\frac{OR - 0.5}{-0.25}\right](R_e)^{+0.9567}(S_h)^{-1.6254}\left(\frac{d_o}{d_p}\right)^{-7.1168} + k\left[\frac{OR - 0.25}{0.25}\right](R_e)^{-2.6560}(S_h)^{+1.1016}\left(\frac{d_o}{d_p}\right)^{0.2063} \quad (36)$$

for $\frac{d_o}{d_p}$ ε [3.4; 6.5]

Figure 8 and Figure 9 show a comparison between the established mathematical models and the experiments performed by Ahmed et al. (2012). Both curves are converging for the two cases for an OR of 0.25 and 0.5. It should be noted that, in the case of an OR of 0.5, the curve of the established model was adjusted by a coefficient of 8.5.

The analytical work to determine the mathematical models is given in Appendix A.

The mathematical model was found to be a strong function of the S_h number, but also of the relative distance from the orifice.

Each model has its advantage and inconvenience in accurately predicting the FAC rate. For example, in Figure 8, the maximum value of the FAC rate for an OR of 0.25 was predicted well, while its position was not.

© University of Pretoria

The size of the OR has been included in the generic model (Figure 10) to enable the use of this model for another OR size between 0.25 and 0.5. Unfortunately, there was no available data for other orifice sizes to be compared with the present generic model (Figure 10). One could see a reduction of FAC increasing the size of the OR (Figure 10).

Figure 8 and Figure 9 show good agreement between the established models and the experimental results of the FAC wear rate. The rate of FAC increases downstream of the orifice and reaches a maximum value in the vicinity of the flow recirculation region.

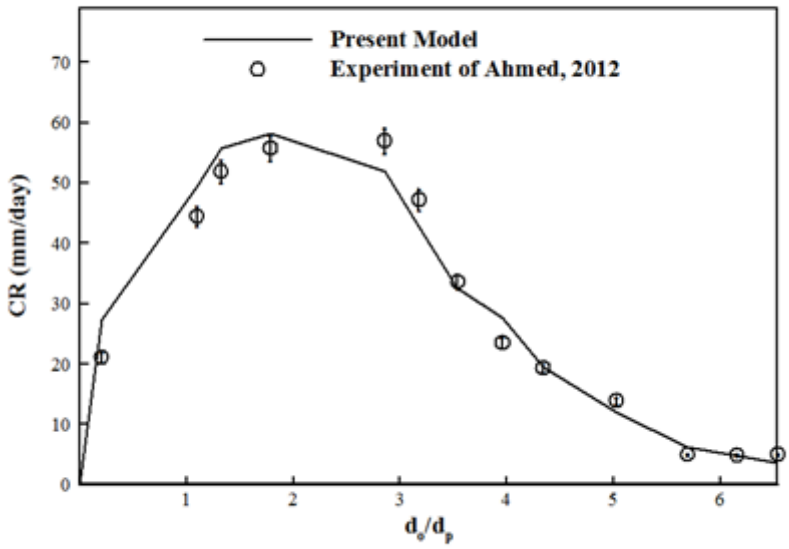

Figure 8. Comparison between modelling and experimental FAC wear rates for an OR of 0.25

© University of Pretoria

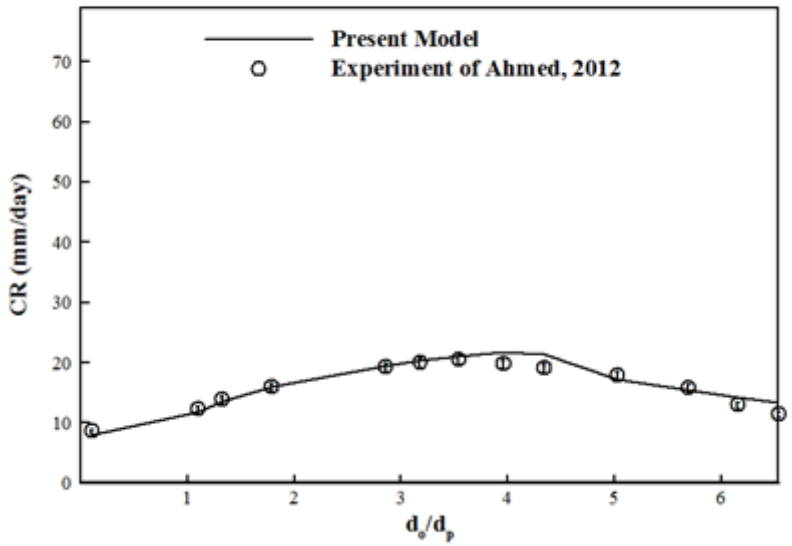

Figure 9. Comparison between modelling and experimental FAC wear rates for an OR of 0.5

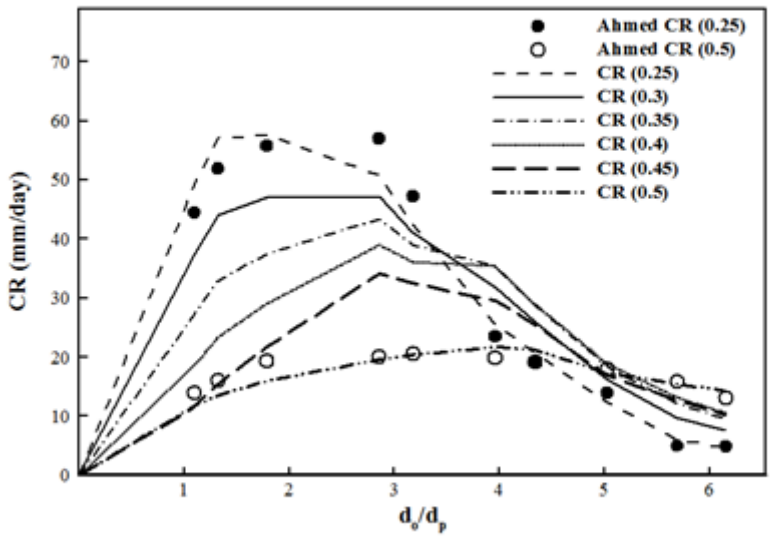

Figure 10. Generic modelling of FAC wear rate for ORs of 0.25, 0.3, 0.35, 0.4, 0.45 and 0.5

© University of Pretoria

5.5 INTERPRETATION OF THE RESULTS

Orifices are commonly used components in piping systems. Mass transfer from the pipe wall to the fluid bulk is enhanced by the flow separation and reattachment downstream of an orifice pipe. This results in an increase in the pipe's CR. Downstream of an orifice, mass and momentum are strengthened by the flow. As a consequence, the mass transfer is enhanced, which gives rise to weak points in the piping system and demands special attention (Nuclear and Industrial Safety Agency 2005). Figure 9 presents the results of the modelling of the FAC wear rate downstream of an OR of 0.25. It is observed that the FAC wear rate increases gradually downstream of the orifice up to a maximum located in the zone $\left(\frac{d_o}{d_p} = 1\ to\ 2\right)$. From there, the FAC wear rate decreases as the flow develops. For the evaluation of FAC downstream of an OR of 0.5 (Figure 10), a similar situation occurs, but the maximum FAC wear rate that is located further downstream between $\frac{d_o}{d_p} = 4\ to\ 5$ decreases thereafter.

The results from the model used to evaluate FAC wear rate for an OR of 0.25 and 0.5 are compared with the experimental data of Ahmed et al. (2012) in Figure 9 and Figure 10. The maximum value of FAC is overpredicted by approximately 2%, while the location of the maximum FAC wear rate is underpredicted by 36% in the case of the flow downstream of the OR of 0.25 (Figure 9). For the case of an OR of 0.5 (Figure 10), the maximum value of the FAC wear rate is overpredicted by 5%, while its position is overpredicted by 11%. In both cases, prediction of the location of the maximum wear rate is within $1\ to\ 5d_p$, which is found to be the same as in a practical situation. The average relative error for the modelling of the value of the FAC wear rate in the case of an OR of 0.25 is about 3%, while for the case of an OR of 0.5, the average is 2%.

© University of Pretoria

Following the previous analysis, one finds that by using the generic model against experimental data, the position of the maximum FAC wear rate for various ORs can be accurately predicted. In the contracted region, FAC wear is underpredicted by the model. This is to be expected in the area of highest velocity with increased oxygen transport across the boundary layer. In areas of flow constriction, velocities increase substantially. Meanwhile, the FAC wear rate is better predicted by the model downstream of the orifice. Where the flow expands, the experimental area downstream of the expansion completely encompasses the recirculation region (Davis and Frawley 2009).

5.6 CONCLUSION

A new mathematical model for FAC was developed. The FAC rate has been correlated as a direct function of the R_e and S_h numbers and the dimensionless distance from the orifice. To simplify the calculation, the R_e number remained unchanged at 20 000, with a flow velocity of 0.71 m per second. Therefore, only the S_h number and the relative distance from the orifice were changed. This resulted in an increase in the FAC rate for smaller ORs and a decrease in the FAC rate for larger orifices.

5.7 RECOMMENDATIONS

The accurate prediction of the FAC rate in this study will require a variable flow velocity and hence different R_e number values. This will lead to tedious calculations that require the use of computational analysis tools. However, with a proper experimental setup, the velocity change, as well as the R_e and S_h numbers, can easily be used as monitors and recorded for a more accurate prediction.

© University of Pretoria

UNIVERSITEIT VAN PRETORIA
UNIVERSITY OF PRETORIA
YUNIBESITHI YA PRETORIA

CHAPTER 6:

CONCLUSION AND RECOMMENDATIONS

© University of Pretoria

6.1 CONCLUSION

An evaluation of the FAC wear rate downstream of an orifice was performed by means of a non-dimensional analysis using the Buckingham Pi theorem. Two cases of orifices were taken into consideration: one with an OR of 0.25 and one with an OR of 0.5. Three dimensionless functions for the FAC wear rate were built and plotted against experimental data. The predictions in the two ORs were in good agreement with the experimental data. The maximum value of the FAC rate was found to increase with a decreasing OR. This maximum value is located between 1 and $5d_p$ downstream of the orifice in both cases. The location's relative distance from the orifice and the S_h number are very important dimensionless parameters that influence the FAC rate downstream of an orifice.

6.2 RECOMMENDATIONS

In summary, this research presented analytical methods that evaluate the rate of corrosion in a pipe downstream of an orifice. This work is expected to support gaining significant means to evaluate the rate of corrosion in pipes. However, it would be more beneficial to cross-check these analytical results with new experimental results. In this work, several experimental works have been attempted, some of which were difficult to interpret, mainly because of the absence of flat surface areas to measure the corrosion rate in the laboratory with conventional methods. It would be interesting to compare the results of the obtained analytical models with new accurate experimental results to obtain greater insights and a better prediction of damages caused by corrosion induced by the flow of water.

The weight loss measurement was not conclusive for this work hence the developed model was correlated with published data of previous experimental works. One way to tackle that barrier is to replace the test section made of mild steel by a test section made of hydrocal; therefore,

© University of Pretoria

instead of measuring the corrosion by weight loss, one will monitor the dissolution of the wall material which occurs by mass transfer from the wall into the bulk flow. The other way could be the utilization of a high resolution camera to take picture during the time and comparing the picture to find the place and progress of the corrosion.

© University of Pretoria

REFERENCES

1. Ahmed, W. H., Bello, M. M., El Nakla, M., Al Sarkhi, A., "Flow and mass transfer downstream of an orifice under flow-accelerated corrosion conditions," *Nuclear Engineering Design*, Vol. 252, 2012, pp. 52–57.

2. Ahmed, W. H., Bello, M. M., Nakla, M. E., "Experimental investigation of flow-accelerated corrosion under two-phase flow conditions," *Nuclear Engineering and Design*, Vol. 267, 2014, pp. 34–43.

3. Ahmed, W. H., "Evaluation of the proximity effect on flow-accelerated corrosion," *Annals of Nuclear Energy*, Vol. 37, No. 8, 2010, pp. 598–605.

4. Ain, A. S., The physical basis of dimensional analysis, *Cambridge: Department of Mechanical Engineering*, MIT., 2001.

5. Ale, S. O., "Encouraging the teaching of mathematical modelling in Nigerian schools," *Nigerian Education Forum*, Vol. 9, No. 2, 1986, pp. 185–191.

6. Ale, S. O, "Curriculum development in modelling process," *International Centre for Theoretical Physics Occasional Publication*, 1981.

7. Berger, F. P., Hue, K. F. F. L., "Mass transfer in turbulent pipe flow measured by the electrochemical method," *International Journal of Heat and Mass Transfer*, Vol. 20, No. 11, 1977, pp. 1185–1194.

8. Bianchi, G., Longhi, P., Mazza, F., ""Horse shoe" corrosion of copper alloys in flowing sea water: mechanism, and possibility of cathodic protection of condenser tubes in power stations," *Corrosion*, Vol. 34, No. 11, 1978, pp. 396-406

© University of Pretoria

9. Boelter, L. M. K., Martinelli, R. C., Jonassen, F., "Remarks on the analogy between heat transfer and momentum transfer," *Transactions of the American Society of Mechanical Engineers*, Vol. 63, 1941, pp. 447-455.

10. Bozzini, B., Ricotti, M. E., Boniardi, M., Mele, C., "Evaluation of erosion-corrosion in multiphase flow via CFD and experimental analysis," *Wear 14th International Conference on Wear of Materials*, Vol. 255, No 1–6, 2003, pp. 237–245.

11. Chen, X., McLaury, B. S., Shirazi, S. A., "A comprehensive procedure to estimate erosion in elbows for gas/liquid/sand multiphase flow," *ASME Journal of Energy Resources Technology*, Vol. 128, No 1, 2005, pp. 70–78.

12. Crawford, N. M., Cunningham, G., Spence, S. W. T., "An experimental investigation into the pressure drop for turbulent flow in 90-degree elbow bends" *Proceedings of the Institution of Mechanical Engineers, Part E: Journal of Process Mechanical Engineering*, Vol. 221, No. 2, pp. 77–88.

13. Davis, C., Frawley, P., "Modelling of erosion-corrosion in practical geometries," *Corrosion Science*, Issue 51, 2009, pp. 769–775.

14. Dhanagal, A., Rajendra, S., Balasubramanian, V., "Influence of pH value, chloride ion concentration and immersion time on corrosion rate of friction stir welded AZ61A magnesium alloy weldments," *Journal of Alloy and Compounds*, Vol. 523, 2012, pp. 49–60.

15. El-Gammal, M., Ahmed, W. H., Ching, C. Y., "Investigation of wall mass transfer characteristics downstream of an orifice," *Nuclear Engineering Design*, Vol. 242, 2012, pp. 353–360.

© University of Pretoria

16. El-Gammal, M., Mazhar, H., Cotton, J. S., Shefski, C., Pietralik, J., Ching, C. Y., "The hydrodynamic effects of single-phase flow on flow-accelerated corrosion in a 90-degree elbow," *Nuclear Engineering Design*, Vol. 240, No. 6, 2010, pp. 1589–1598.

17. Fage, A.,Townend, H. C. H, "An examination of turbulent flow with an ultramicroscope," *Proceedings of the Royal Society of London*, Vol. 135, No. 828, pp. 656-677

18. Gasem, Z. M., "Chapter#5 Polarization methods for corrosion rate measurements," *ME472 King Fahd University of Petroleum & Minerals (KFUPM)*, 2011, pp.01-25.

19. Harriott, P., Hamilton, R. M., "Solid-liquid mass transfer in turbulent pipe flow," *Chemical Engineering Science*, 1965, pp. 1073-1078.

20. Hewitt, G. F., *Measurement of two-phase flow parameters*, London, Academic Press, 1978.

21. Isaacs, H. S., Vyas, B., "Scanning electrode techniques in localized corrosion," In: F. M. &. U. Bertocci ed., *Electrochemichal corrosion testing ASTM STP 727*. s.l., American Society for Testing and Materials, 1981, pp. 3–33.

22. Jepson, W. P., "Modelling the transition to slug flow in horizontal conduit," *The Canadian Journal of Chemical Engineering*, Vol. 67, No. 5, 1989, pp. 731–740.

23. Karman, T. V., " The analogy between fluid friction and heat transfer," 1939. *Transactions of the American Society of Mechanical Engineers*, Vol. 61, p. 705.

24. Kastner, W., Erve, M., Henzel, N., Stellwag, B., "Calculation code for erosion corrosion-induced wall thinning in piping systems," *Nuclear Engineering and Design*, Vol. 119, No. 2–3, 1990, pp. 431–438.

© University of Pretoria

25. Keating, A., Nesic, S., "Prediction of two-phase erosion-corrosion in bends," *Second International Conference on CFD in the Mineral and Process Industries*, Melbourne, 1999.

26. Kim, S., Park, J. H., Kojasoy, G., Kelly, J. M., Marshall, S. O., "Geometric effects of 90-degree elbow in the development of interfacial structures in horizontal bubbly flow," *Nuclear Engineering and Design*, Vol. 237, 2007, pp. 2105–2113.

27. Levich, V .G., *Physiochemical hydrodynamics*, New Jersey, Englewood Cliffs, 1962.

28. Liang, J., Deng, A., Xie, R., Gomez, M., Hu, J., Zhang, J., Ong, C. N., Adin, A., "Impact of flow rate on corrosion of cast iron and quality of re-mineralized seawater reverse osmosis (SWRO) membrane product water," *Desalination*, Vol. 322, 2013, pp. 76–83.

29. Lin, C. S., Moulton, R. W., Putnam, G. L., "Mass transfer between solid and fluid streams," *Engineering and Process Development*, Vol. 45, No. 3, 1953, pp. 636–640.

30. Linton, W. H., Sherwood, T. K., "Mass transfer from solid shapes to water in streamline and turbulent flow," *Chemical Engineering Progress*, Vol. 46, 1950, pp. 258–264.

31. Lotz, U., Postlethwaite, J., "Erosion-corrosion in disturbed two-phase liquid particle flow," *Corrosion*, Vol. 30, No. 1, 1990, pp. 95–106.

32. Ma, K. T., Ferng, Y. M., Ma, Y. P., "Numerically investigating the influence of local flow behaviors on flow-accelerated corrosion using two-fluid equations," *Materials for Nuclear Systems*, Vol. 123, No. 1, 1998, pp. 90–102.

33. Manmatha, K. R., Sukanta, K. D., "Single-phase and two-phase flow through thin and thick orifices in horizontal pipes," *ASME Journal of Fluids Engineering*, Vol. 134, No. 9, 2012, pp. 1–14.

© University of Pretoria

34. Massey, B., *Mechanics of Fluids*, 8th ed., London, Taylor & Francis, 2006.

35. Nesic, S., Postlethwaite, J., "Hydrodynamics of disturbed flow and erosion-corrosion. Part I – single-phase flow study," *The Canadian Journal of Chemical Engineering*, Vol. 69, No. 3, 1991, pp. 698–703.

36. Nesic, S., Postlethwaite, J., "Hydrodynamics of the disturbed flow and erosion-corrosion. Part II – two-phase flow study," *The Canadian Journal of Chemical Engineering*, Vol. 69, No. 3, 2009, pp. 704–710.

37. Nuclear and Industrial Safety Agency, "Secondary piping rupture accident at Mihama power station, unit 3, of the Kansai Electric Power Co., Inc. (final report)," *Japan Nuclear Energy Safety Organisation*, 2005.

38. Petric, G. W., Ksiazek, P. E., "Flow-accelerated corrosion in industrial steam and powerplants," *Engineering and Papermakers Conference*, 1997.

39. Pietralik, J. M., Schefski, C. S., "Flow and mass transfer in bends under FAC wall thinning conditions," *17th International Conference on Nuclear Energy*, Brussels, 2009a, p. 9.

40. Pietralik, J. M., Schefski, C. S., "Flow and mass transfer in bends under flow-accelerated corrosion wall thinning conditions," *Journal of Engineering for Gas Turbines and Power*, Vol. 133, No. 1, 2009b.

41. Pietralik, J. M., Schefski, C. S., "Flow and mass transfer in bends under flow-accelerated corrosion wall thinning conditions," 1*7th International Conference on Nuclear Engineering*, Vol. 1, 2009c, pp. 493–501

© University of Pretoria

42. Pietralik, J. M., Smith, B. A. W., "CFD application to flow-accelerated corrosion in feeder bends," *14th International Conference on Nuclear Energy*, Miami, 2006, pp. 175–185.

43. Postlethwaite, J., Dobbin, M. H., Bergevin, K., "The role of oxygen mass transfer in the erosion-corrosion of slurry pipelines," *Corrosion*, Vol. 42, No. 9, 1985, pp. 514–521.

44. Poulson, B., Greenwell, B. S., Chexal, B., Horowitz, G., "Modelling hydrodynamic parameters to predict flow-assisted corrosion-water reactors," *Proceedings of the 5th International Conference on Environmental Degradation of Materials in Nuclear Power Systems, American Nuclear Society*, La Grange Park, 1992.

45. Poulson, B., Robinson, R., "The local enhancement of mass transfer at 180-degree bends," *International Journal of Heat and Mass Transfer*, Vol. 31, No. 6, 1988, pp. 1289–1297.

46. Poulson, B., "Predicting the occurence of erosion corrosion". In: J. R. Nichols, ed., *Plant corrosion: prediction of materials performance*, Chichester, Ellis Harwood, 1987, pp. 101–132.

47. Poulson, B., "Measuring and modelling mass transfer at bends in annular two-phase flow," *Chemical Engineering Science*, Vol. 46, No. 4, 1991, pp. 1069–1082.

48. Poulson, B., "Complexities in predicting erosion corrosion," *Wear*, Vol. 497–504 , 1999, pp. 233–235.

49. Poulson, B., "Electrochemichal measurements in flowing solutions," *Corrosion Science*, Vol. 23, No. 4, 1983, pp. 391–430.

© University of Pretoria

50. Poulson, B., "Predicting and preventing flow-accelerated corrosion in nuclear power plant," *International Journal of Nuclear Energy*, 2014.

51. Prandtl, L., " Heat convection in a tube," *Physikalisch Zeitschrift*, Vol. 29, 1928, p.487

52. Reichardt, H., "Heat transfer through turbulent friction layers," N*ational Advisory Committee for Aeronautics*, technical memorandum No. 1047, 1943.

53. Robinson, J., Drews, T., *Resolving flow-accelerated corrosion problems in the industrial steam plant*, TX USA, BetzDearborn, 1999.

54. Sarmasti, E. M. R., "Mathematical modelling of corrosion phenomenon in pipelines," *The Journal of Mathematics and Computer Science*, Vol. 3, No. 2, 2011, pp. 202–211.

55. Schweitzer, P. A, "Fundamentals of metallic corrosion (atmospheric and media corrosion of metals)," *Corrosion Engineering Handbook*, 2nd ed., CRC Press, 2007.

56. Shreir, L. L., Jarman, R. A., Burstein, G. T., *Corrosion, Oxford; Boston: Butterworth-Heinemann*, 1994.

57. Sydberger, T., Lotz, U., "Relation between mass transfer and corrosion in a turbulent pipe flow," *Journal of Electrochemichal Society*, Vol. 129, No. 2, 1982, pp. 276–283.

58. *Taylor, G. I., "*Conditions at the surface of a hot body exposed to the wind,*" Great Britain Advisory Committee for Aeronautics, Reports and Memoranda, Vol. 2, No. 272, 1916-1917, pp. 423-429.*

59. Tong, H. S., "Corrosion and electrochemical behavior of iron-chromium-nickel alloys in concentrated sulfuric acid solutions," *Symposium on Progress in Electrochemical Corrosion Testing, American Society for Testing and Materials, 1979, pp. 20-25.*

© University of Pretoria

60. Tousek, J., "Potential dependence of localized corrosion in iron, " In: F. Mansfield and U. Bertocci, ed., *Electrochemichal corrosion testing ASTM STP 727,* American Society for Testing and Materials, 1981, pp. 34–42.

61. Turnbull, I. A., Robinson, M. J., "Investigation into boiler corrosion on the historic vessel SL Dolly," *Corrosion Engineering Science and Technology,* Vol. 40, No 2, 2005, pp. 143–148.

62. Uchida, S., Naitoh, M., Uehara, Y., Okada, H., and Lister, D. H., "Evaluation method for flow accelerrate corrosion of components by corrosion analysis coupled with flow dyniamics analysis," *13th International Conference on Environmental Degradation of Materials in Nuclear Power Systems,* Whistler, 2007.

63. Uchida, S., "Evaluation method for FAC of components by corrosion analysis coupled with flow dynamics analysis," *Proceedings of the Annual Meeting of the Executive Committee and Working Groups of the International Association for the Properties of Water and Steam,* Witney, 2006.

64. Wang, D., "Characterization of local mass transfer rate downstream of an orifice," *MacMaster University,* 2012.

65. Wharton, J. A., Wood, R. J. K., "Influence of flow conditions on the corrosion of AISI 304L stainless steel," *Wear,* Vol. 256, pp. 525-536.

66. Wraag, A. A., "Applications of the limiting diffusion current technique in chemical engineering," *Chemical Engineer,* Vol. 316, 1977, pp. 39–49.

67. Yamagata, T., Ito, A., Sato, Y., Fujisawa, N., "Experimental and numerical studies on mass transfer characteristics behind an orifice in a circular pipe for application to

© University of Pretoria

pipe-wall thinning," *Experimental Thermal and Fluid Science*, Issue 52, 2014, pp. 239-247.

68. Yoneda, K., "Evaluation of hydraulic factors affecting flow accelerated corroson and its verification with power plant data," *ASME Pressure Vessels and Piping Conference*, Prague, Vol. 6, 2009.

69. Yurmanov V., Rakhmanov A., " Flow accelerated corrosion of pipelines and equipment at Russian nuclear power plants: problems and solutions," *International Atomic Energy* Agency, *workshop on erosion-corrosion including flow-accelerated corrosion and environmentally assisted cracking issues in nuclear power plants, Moscow*, 2009.

70. Zinemans, D., Herszaz, A., "Flow-accelerated corrosion: flow field and mass transport in bifurcations and nozzles," *International Conference on Water Chemistry for Nuclear Reactor Systems*, Berlin, 2008.

71. Zheng, D., Che, D., Liu, Y., "Experimental investigation on gas-liquid two-phase slug flow enhanced carbon dioxide corrosion in vertical upward pipeline," *Corrosion Science*, Issue 50, 2008, pp. 3005-3020.

© University of Pretoria

APPENDIX

A. DERIVATION OF THE EQUATIONS

$$CR = f(u, \rho, \mu, D, d_o, C, d_p, \Delta P, \Delta T, g) \tag{37}$$

Table 4. SI units

Quantity	**SI name**	**SI symbol**
Length (L)	metre	m
Time (t)	second	s
Mass (M)	kilogram	kg
Temperature (T)	kelvin	K
Current (I)	ampere	A
Number of elementary particles	mole	mol
Luminous intensity	candela	cd

Quantity	**Defining equation law**	**Dimension**	**Dimensional symbol**	**Name**
Area	$A=\int dxdy$	L^2	m^2	- - -
Volume	$V=\int dxdydz$	L^3	m^2	- - -
Frequency	$f=l/\tau$	t^{-1}	m^2	hertz (Hz)
Velocity	$v=dx/dt$	Lt^{-1}	m^3	- - -
Acceleration	$a=d^2x/dt^2$	Lt^{-2}	s^{-1}	- - -
Density	$\rho=M/V$	ML^{-3}	ms^{-1}	- - -
Force	$F=Ma$	MLt^{-2}	$kg\ m^{-3}$	newton (N)
Stress/pressure	$p=F/A$	$ML^{-1}t^{-2}$	$kg\ ms^{-2}$	pascal (Pa)
Work/energy	$W=\int Fdx$	ML^2t^{-2}	$N\ m^{-2}=kg\ m^{-1}s^{-2}$	joule (J)
Torque	$T=Fl$	ML^2t^{-2}	$N\ m=kg\ m^2s^{-2}$	- - -
Power	dW/dt	ML^2t^{-3}	$J\ s^{-1}=kg\ m^2s^{-3}$	watt (W)
Charge	$Q=\int Idt$	It	$A\ s$	coulomb (C)

© University of Pretoria

where the primary dimensions of each parameters are listed below:

CR = Corrosion rate $\{CR\} = \{Lt^{-1}\}$ or $\{CR\} = \{L^2t^{-1}\}$

u = Fluid velocity with $\{u\} = \{Lt^{-1}\}$

ρ = Fluid density with $\{\rho\} = \{ML^{-3}\}$

μ = Fluid viscosity with $\{\mu\} = \{ML^{-1}t^{-1}\}$

D = Mass diffusivity with $\{D\} = \{L^2t^{-1}\}$

d_o = Distance from orifice $\{d_o\} = \{L\}$

C = Concentration of species with $\{C\} = \{NL^{-3}\}$

d_p = Pipe diameter $\{d_p\} = \{L\}$

ΔP = Pressure difference $\{\Delta P\} = \{Mt^{-2}L^{-1}\}$

ΔT = Temperature variation $\{\Delta T\} = \{T\}$

g = Gravitational force $\{g\} = \{Lt^{-2}\}$

There are five primary dimensions and, with the method of repeating variables, the reduction was chosen as $j = 6$, which implies that 6 π_S' groups will have to be established, defined as follows:

$$\pi_1 = f(\pi_2, \pi_3, \pi_4, \pi_5, \pi_6) \tag{38}$$

with

π_1: Dependent π group

$\pi_2 \ldots \pi_6$: Independent π groups

© University of Pretoria

A.1. METHOD OF REPEATING VARIABLES

The repeating variables chosen were d_p, u , ρ , C and ΔT and $\{CR\} = \{Lt^{-1}\}$.

Therefore:

$$\{\pi_1\} = \left\{CR d_p^{a_1} u^{b_1} \rho^{c_1} C^{d_1} (\Delta T)^{e_1}\right\}$$

$$= \{(Lt^{-1})(L^{a_1})(Lt^{-1})^{b_1}(ML^{-3})^{c_1}(NL^{-3})^{d_1}(T)^{e_1}\} \quad (39)$$

$$= \{L^0 t^0 M^0 N^0 T^0\}$$

Then,

$$a_1 = 0;\ b_1 = -1\ ;\ c_1 = 0\ ;d_1 = 0 \text{ and } e_1 = 0$$

Thus,

$$\pi_1 = \frac{CR}{u} \quad (40)$$

$$\{\pi_2\} = \left\{\mu d_p^{a_2} u^{b_2} \rho^{c_2} C^{d_2} (\Delta T)^{e_2}\right\}$$

$$= \{(ML^{-1}t^{-1})(L^{a_2})(Lt^{-1})^{b_2}(ML^{-3})^{c_2}(NL^{-3})^{d_2}(T)^{e_2}\} \quad (41)$$

$$= \{L^0 t^0 M^0 N^0 T^0\}$$

Then,

$a_2 = -1;\ b_2 = -1\ ;\ c_2 = -1\ ;\ d_2 = 0$ and $e_2 = 0$

Thus,

$$\pi_2 = \frac{\mu}{\rho u d_p} = \frac{1}{R_e} \quad (42)$$

© University of Pretoria

$$\{\pi_3\} = \left\{D d_p^{a_3} u^{b_3} \rho^{c_3} C^{d_3} (\Delta T)^{e_3}\right\}$$

$$= \{(L^2 t^{-1})(L^{a_3})(Lt^{-1})^{b_3}(ML^{-3})^{c_3}(NL^{-3})^{d_3}(T)^{e_3}\} \quad (43)$$

$$= \{L^0 t^0 M^0 N^0 T^0\}$$

Then,

$a_3 = -1;\ b_3 = -1\ ;\ c_3 = 0; d_3 = 0$ and $e_3 = 0$

Thus,

$$\pi_3 = \frac{D}{u d_p} = \frac{1}{S_h} \quad (44)$$

$$\{\pi_4\} = \left\{d_o d_p^{a_4} u^{b_4} \rho^{c_4} C^{d_4} (\Delta T)^{e_4}\right\} = \{(L)(L^{a_4})(Lt^{-1})^{b_4}(ML^{-3})^{c_4}(NL^{-3})^{d_4}(T$$

$$= \{L^0 t^0 M^0 N^0 T^0\} \quad (45)$$

Then,

$a_4 = -1; b_4 = 0\ ; c_4 = 0; d_4 = 0$ and $e_4 = 0$

Thus,

$$\pi_4 = \frac{d_o}{d_p} \quad (46)$$

$$\{\pi_5\} = \left\{\Delta P d_p^{a_5} u^{b_5} \rho^{c_5} C^{d_5} (\Delta T)^{e_5}\right\}$$

$$= \{(Mt^{-2}L^{-1})(L^{a_5})(Lt^{-1})^{b_5}(ML^{-3})^{c_5}(NL^{-3})^{d_5}\} \quad (47)$$

$$= \{L^0 t^0 M^0 N^0 T^0\}$$

Then,

$a_5 = 0; b_5 = -2\ ; c_5 = -1; d_5 = 0$ and $e_5 = 0$

© University of Pretoria

Thus,

$$\pi_5 = \frac{\Delta P}{\rho u^2} = Eu \tag{48}$$

$$\{\pi_6\} = \left\{g d_p^{a_6} u^{b_6} \rho^{c_6} C^{d_6} (\Delta T)^{e_6}\right\}$$

$$= \{(Mt^{-2}L^{-1})(L^{a_6})(Lt^{-1})^{b_6}(ML^{-3})^{c_6}(NL^{-3})^{d_6}\} \tag{49}$$

$$= \{L^0 t^0 M^0 N^0 T^0\}$$

Then,

$a_6 = 1$; $b_6 = -2$; $c_6 = 0$; $d_6 = 0$ and $e_6 = 0$

Thus,

$$\pi_6 = \frac{g D_p}{u^2} \cong \frac{u}{\sqrt{g D_p}} = F_r \tag{50}$$

Finally, we yield to the following function:

$$\frac{CR}{u} = f\left(\frac{1}{R_e}, \frac{1}{S_h}, \frac{d_o}{d_p}, Eu, F_r\right) \tag{51}$$

Neglecting $Eu, F_{r,}$ we yield to:

$$\frac{CR}{u} = f\left(\frac{1}{R_e}, \frac{1}{S_h}, \frac{d_o}{d_p}\right) \tag{52}$$

Now we will attempt to build a function as per the above non-dimensional mathematical model.

$$\frac{CR}{u} = (R_e)^{-a}(S_h)^{-b}\left(\frac{d_o}{d_p}\right)^c \tag{53}$$

We will use the data from the study proposed by Ahmed et al. (2012) for an OR of 0.25 and 0.5.

Note: $u = 0.71\frac{m}{s}$ And $R_e = 20000$

© University of Pretoria

A.2. CASE 1: ORIFICE RATIO 0.25

$$\frac{50.42}{u} = (20000)^{-a_1}(3218)^{-b_1}(1.2)^{c_1}$$

$$\frac{55.3}{u} = (20000)^{-a_1}(5306)^{-b_1}(1.6)^{c_1}$$

$$\frac{36.92}{u} = (20000)^{-a_1}(8976)^{-b_1}(3.4)^{c_1}$$

$$\frac{20.07}{u} = (20000)^{-a_2}(5568)^{-b_2}(4.3)^{c_2}$$

$$\frac{6.24}{u} = (20000)^{-a_2}(3371)^{-b_2}(5.7)^{c_2}$$

$$\frac{5.03}{u} = (20000)^{-a_2}(2590)^{-b_2}(6.5)^{c_2}$$

$$\frac{1.18}{u} = (20000)^{-a_3}(2166)^{-b_3}(7.4)^{c_3}$$

$$\frac{1.01}{u} = (20000)^{-a_3}(1903)^{-b_3}(8.1)^{c_3}$$

$$\frac{2.97}{u} = (20000)^{-a_3}(1490)^{-b_3}(9.7)^{c_3}$$

$$\frac{2.21}{u} = (20000)^{-a_b}(1489)^{-b_b}(10)^{c_b}$$

© University of Pretoria

A.2.1. SOLUTION OF THE EQUATIONS FOR AN ORIFICE RATIO OF 0.25

$$\frac{5.83.10^{-7}}{u} = (20000)^{-a_1}(3218)^{-b_1}(1.2)^{c_1}$$

$$\frac{6.4.10^{-7}}{u} = (20000)^{-a_1}(5306)^{-b_1}(1.6)^{c_1}$$

$$\frac{4.27.10^{-7}}{u} = (20000)^{-a_1}(8976)^{-b_1}(3.4)^{c_1}$$

$$\begin{cases} \frac{5.83.10^{-7}}{u} = (20000)^{-a_1}(3218)^{-b_1}(1.2)^{c_1} \\ \frac{6.4.10^{-7}}{u} = (20000)^{-a_1}(5306)^{-b_1}(1.6)^{c_1} \\ \frac{4.27.10^{-7}}{u} = (20000)^{-a_1}(8976)^{-b_1}(3.4)^{c_1} \end{cases}$$

$$\Rightarrow \begin{cases} (20000)^{-a_1}(3218)^{-b_1}(1.2)^{c_1} = \frac{5.83.10^{-7}}{u} = \frac{5.83.10^{-7}}{0.71} = 8.21 \times 10^{-7} = A \\ (20000)^{-a_1}(5306)^{-b_1}(1.6)^{c_1} = \frac{6.4.10^{-7}}{0.71} = \frac{6.40.10^{-7}}{u} = 9.01 \times 10^{-7} = B \\ (20000)^{-a_1}(8976)^{-b_1}(3.4)^{c_1} = \frac{4.27.10^{-7}}{0.71} = \frac{4.27.10^{-7}}{0.71} = 6.01 \times 10^{-7} = C \end{cases}$$

$$\Rightarrow \begin{cases} (20000)^{-a_1}(3218)^{-b_1}(1.2)^{c_1} = A \\ (20000)^{-a_1}(5306)^{-b_1}(1.6)^{c_1} = B \\ (20000)^{-a_1}(8976)^{-b_1}(3.4)^{c_1} = C \end{cases}$$

$$\Rightarrow \begin{cases} ln[(20000)^{-a_1}(3218)^{-b_1}(1.2)^{c_1}] = ln(A) \\ ln[(20000)^{-a_1}(5306)^{-b_1}(1.6)^{c_1}] = ln(B) \\ ln[(20000)^{-a_1}(8976)^{-b_1}(3.4)^{c_1}] = ln(C) \end{cases}$$

$$\Rightarrow \begin{cases} ln[(20000)^{-a_1}] + ln[(3218)^{-b_1}] + ln[(1.2)^{c_1}] = ln(A) \\ ln[(20000)^{-a_1}] + ln[(5306)^{-b_1}] + ln[(1.6)^{c_1}] = ln(B) \\ ln[(20000)^{-a_1}] + ln[(8976)^{-b_1}] + ln[(3.4)^{c_1}] = ln(C) \end{cases}$$

$$\Rightarrow \begin{cases} -a_1 ln(20000) - b_1 ln(3218) + c_1 ln(1.2) = ln(A) \\ -a_1 ln(20000) - b_1 ln(5306) + c_1 ln(1.6) = ln(B) \\ -a_1 ln(20000) - b_1 ln(8976) + c_1 ln(3.4) = ln(C) \end{cases}$$

© University of Pretoria

$$\Rightarrow \begin{cases} -9.90a_1 - 8.08b_1 + 0.18c_1 = ln(A) = \ln(8.21 \times 10^{-7}) = -14.013 \\ -9.90a_1 - 8.58b_1 + 0.47c_1 = ln(B) = \ln(9.01 \times 10^{-7}) = -13.92 \\ -9.90a_1 - 9.10b_1 + 1.22c_1 = ln(C) = \ln(6.01 \times 10^{-7}) = -14.325 \end{cases}$$

$$\Rightarrow \begin{bmatrix} -9.90 & -8.08 & 0.18 \\ -9.90 & -8.53 & 0.47 \\ -9.90 & -9.10 & 1.22 \end{bmatrix} \times \begin{bmatrix} a_1 \\ b_1 \\ c_1 \end{bmatrix} = \begin{bmatrix} -14.013 \\ -13.92 \\ -14.325 \end{bmatrix}$$

$$\Rightarrow A.X = B$$

With

$$A = \begin{bmatrix} -9.90 & -8.08 & 0.18 \\ -9.90 & -8.53 & 0.47 \\ -9.90 & -9.10 & 1.22 \end{bmatrix}; X = \begin{bmatrix} a_1 \\ b_1 \\ c_1 \end{bmatrix}; B = \begin{bmatrix} -14.013 \\ -13.92 \\ -14.325 \end{bmatrix}$$

$$\begin{cases} a_1 = \dfrac{detA_1}{\det A} \\ b_1 = \dfrac{detA_2}{\det A} \\ c_1 = \dfrac{detA_3}{\det A} \end{cases}$$

With

$$A = \begin{bmatrix} -9.90 & -8.08 & 0.18 \\ -9.90 & -8.53 & 0.47 \\ -9.90 & -9.10 & 1.22 \end{bmatrix}; A_1 = \begin{bmatrix} -14.013 & -8.08 & 0.18 \\ -13.920 & -8.53 & 0.47 \\ -14.325 & -9.10 & 1.22 \end{bmatrix};$$

$$A_2 = \begin{bmatrix} -9.90 & -14.013 & 0.18 \\ -9.90 & -13.920 & 0.47 \\ -9.90 & -14.325 & 1.22 \end{bmatrix}; A_3 = \begin{bmatrix} -9.90 & -8.08 & -14.013 \\ -9.90 & -8.53 & -13.920 \\ -9.90 & -9.10 & -14.325 \end{bmatrix}$$

Recall:

$$A = \begin{bmatrix} a_{11} & a_{12} & a_{13} \\ a_{21} & a_{22} & a_{23} \\ a_{31} & a_{32} & a_{33} \end{bmatrix}$$

$$\boldsymbol{\det A = a_{12}C_{12} + a_{22}C_{22} + a_{32}C_{32}}$$

© University of Pretoria

With the cofactor, C_{ij} of a matrix A defined by the relationship:

$$\boldsymbol{C_{ij}} = (-\mathbf{1})^{i+j}\boldsymbol{M_{ij}}$$

The minor M_{ij} is the determinant of the obtained matrix by eliminating the i^{n+1} line of the j^{n+1} column of A.

For more accuracy of the results, we used MATLAB 7.11.0.

$$det(A) = det\left(\begin{bmatrix} -9.90 & -8.08 & 0.18 \\ -9.90 & -8.53 & 0.47 \\ -9.90 & -9.10 & 1.22 \end{bmatrix}\right) = 1.7048$$

$$det(A_1) = det\left(\begin{bmatrix} -14.013 & -8.08 & 0.18 \\ -13.920 & -8.53 & 0.47 \\ -14.325 & -9.10 & 1.22 \end{bmatrix}\right) = 3.8833$$

$$det(A_2) = det\left(\begin{bmatrix} -9.90 & -14.013 & 0.18 \\ -9.90 & -13.920 & 0.47 \\ -9.90 & -14.325 & 1.22 \end{bmatrix}\right) = -1.8533$$

$$det(A_3) = det\left(\begin{bmatrix} -9.90 & -8.08 & -14.013 \\ -9.90 & -8.53 & -13.920 \\ -9.90 & -9.10 & -14.325 \end{bmatrix}\right) = -2.3291$$

$$\begin{cases} a_1 = \dfrac{3.8833}{1.7048} \\ b_1 = \dfrac{-1.8533}{1.7048} \\ c_1 = \dfrac{-2.3291}{1.7048} \end{cases} \Rightarrow \begin{cases} a_1 = 2.2779 \\ b_1 = -1.0871 \\ c_1 = -1.3662 \end{cases}$$

$$\boldsymbol{Therefore:} \begin{cases} \boldsymbol{a_1 = 2.2779} \\ \boldsymbol{b_1 = -1.0871} \\ \boldsymbol{c_1 = -1.3662} \end{cases} \begin{cases} \boldsymbol{a_2 = -0.9567} \\ \boldsymbol{b_2 = 1.6254} \\ \boldsymbol{c_2 = -7.1168} \end{cases} \begin{cases} \boldsymbol{a_3 = 89.8862} \\ \boldsymbol{b_3 = -76} \\ \boldsymbol{c_3 = 107.7778} \end{cases}$$

$$\frac{CR}{u} = (R_e)^{-2.2779}(S_h)^{+1.0871}\left(\frac{d_o}{d_p}\right)^{-1.3662} \quad \text{For } \frac{d_o}{D_p} \in [0; 3.4] \qquad (18)$$

$$\frac{CR}{u} = (R_e)^{+0.9567}(S_h)^{-1.6254}\left(\frac{d_o}{d_p}\right)^{-7.1168} \quad \text{For } \frac{d_o}{D_p} \in [3.4; 6.5] \qquad (19)$$

© University of Pretoria

A.3. CASE 2: ORIFICE RATIO 0.5

$$\frac{13}{u} = (20000)^{-a_1}(2771)^{-b_1}(1.2)^{c_1}$$

$$\frac{15.35}{u} = (20000)^{-a_1}(3094)^{-b_1}(1.6)^{c_1}$$

$$\frac{21.2}{u} = (20000)^{-a_1}(3572)^{-b_1}(3.4)^{c_1}$$

$$\frac{19.55}{u} = (20000)^{-a_2}(3515)^{-b_2}(4.3)^{c_2}$$

$$\frac{16.08}{u} = (20000)^{-a_2}(2477)^{-b_2}(5.7)^{c_2}$$

$$\frac{12.05}{u} = (20000)^{-a_2}(2254)^{-b_2}(6.5)^{c_2}$$

$$\frac{8.67}{u} = (20000)^{-a_3}(1907)^{-b_3}(7.4)^{c_3}$$

$$\frac{5.73}{u} = (20000)^{-a_3}(1775)^{-b_3}(8.1)^{c_3}$$

$$\frac{3.63}{u} = (20000)^{-a_3}(1528)^{-b_3}(9.7)^{c_3}$$

$$\frac{3.26}{u} = (20000)^{-a_b}(1508)^{-b_b}(10)^{c_b}$$

A.3.1. SOLUTION OF THE EQUATIONS FOR AN ORIFICE RATIO OF 0.5

$$\boldsymbol{Therefore:} \begin{cases} \boldsymbol{a_1 = 2.6560} \\ \boldsymbol{b_1 = -1.1016} \\ \boldsymbol{c_1 = 0.2063} \end{cases} \quad \begin{cases} \boldsymbol{a_2 = -1.5202} \\ \boldsymbol{b_2 = 2.7833} \\ \boldsymbol{c_2 = -4.1576} \end{cases} \quad \begin{cases} \boldsymbol{a_3 = 1.1204} \\ \boldsymbol{b_3 = 0.0846} \\ \boldsymbol{c_3 = -2.5705} \end{cases}$$

$$\frac{CR}{u} = k(R_e)^{-2.6560}(S_h)^{+1.1016}\left(\frac{d_o}{d_p}\right)^{0.2063} \qquad \text{For } \frac{d_o}{d_p} \varepsilon [0; 6.5] \qquad (20)$$

Note: Always use the correction factor k = 8.5 for an OR model of 0.5.

© University of Pretoria